

# PipeMare: Asynchronous Pipeline Parallel DNN Training

Bowen Yang<sup>1</sup>, Jian Zhang<sup>1,2</sup>, Jonathan Li<sup>1</sup>,  
Christopher Ré<sup>1,2</sup>, Christopher R. Aberger<sup>1,2</sup>, and Christopher De Sa<sup>1,3</sup>

<sup>1</sup>SambaNova Systems

<sup>2</sup>Department of Computer Science, Stanford University

<sup>3</sup>Department of Computer Science, Cornell University

`bowen.yang@sambanovasystems.com, zjian@stanford.edu, jlli@stanford.edu,`  
`christopher.aberger@sambanovasystems.com, chrismre@cs.stanford.edu,`  
`cdesa@cs.cornell.edu`

## Abstract

Recently there has been a flurry of interest around using pipeline parallelism while training neural networks. Pipeline parallelism enables larger models to be partitioned spatially across chips and within a chip, leading to both lower network communication and overall higher hardware utilization. Unfortunately, to preserve statistical efficiency, existing pipeline-parallelism techniques sacrifice hardware efficiency by introducing bubbles into the pipeline and/or incurring extra memory costs. In this paper, we investigate to what extent these sacrifices are necessary. Theoretically, we derive a simple but robust training method, called PipeMare, that tolerates asynchronous updates during pipeline-parallel execution. Using this, we show empirically, on a ResNet network and a Transformer network, that PipeMare can achieve final model qualities that match those of synchronous training techniques (at most 0.9% worse test accuracy and 0.3 better test BLEU score) while either using up to  $2.0\times$  less weight and optimizer memory or being up to  $3.3\times$  faster than other pipeline parallel training techniques. To the best of our knowledge we are the first to explore these techniques and fine-grained pipeline parallelism (e.g. the number of pipeline stages equals to the number of layers) during neural network training.

## 1 Introduction

In the past several years there has been an explosion of interest in hardware chips designed for training deep neural networks [6, 20, 10, 21]. These works posit that the traditional mechanisms used to train neural networks are wildly inefficient and that orders of magnitude performance speedups can be had by rethinking the process entirely. One of the central ideas that has emerged out of this effort is that model parallelism can be leveraged in place of, or in addition to, the standard data parallelism. The key idea here is to partition neural network layers spatially across hardware resources while pipelining the computation between them. Training a neural network in this model-parallel fashion is what we call *pipeline parallelism*.

There are several inherent benefits of pipeline parallelism over traditional data parallel execution. First, it *eliminates context switching*. GPUs run neural network training on a kernel-by-kernel basis, meaning that each new low-level operator or kernel must be dynamically dispatched from the CPU to GPU: this dispatch time (or context switching time) can be costly. With pipeline parallelism, operators are spatially fixed across compute resources and the entire computation graph is able to run as a single context (i.e. no dynamic dispatching). Second, pipeline parallelism *alleviates the accelerator memory bottleneck*. When training deep neural networks (DNNs) with a kernel-by-kernel accelerator, activations and weights must continually be marshaled back and forth to main memory, which can be a bottleneck (even in the distributed setting, as

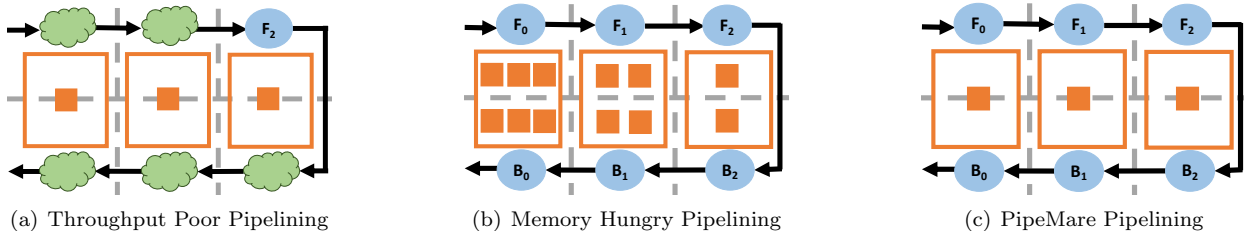


Figure 1: Different extremes of pipelining modes. The orange squares represent model weight memory, the blue circles represent active pipeline compute, the green clouds represent pipeline bubbles, and the dashed gray lines represent different pipeline stages. Throughput poor pipelining (a) keeps one copy of weight memory but inserts bubbles which cause pipeline stalls. Memory hungry pipelining (b) does not have pipeline stalls but uses additional copies of weight memory. The number of bubbles in (a) and the number of weight copies in (b) increases linearly with the number of pipeline stages, forcing an increased cost of either throughput or memory. PipeMare (c) fully utilizes the compute pipeline (no stalls) while minimizing the weight memory footprint. GPipe is one type of throughput Poor Pipelining because it has bubbles in the pipeline execution. PipeDream is one type of memory hungry pipelining because it needs to maintain multiple copies of model weights.

the weight memory is replicated across all the devices). This problem is only getting worse as state-of-the-art models are becoming larger across domains [13, 18, 23]. Pipeline parallelism alleviates this memory bottleneck in a distributed setting by splitting up the weights (and therefore not replicating them as in data parallelism) across accelerators. Third, others [7] have shown that pipeline parallelism can *reduce network bandwidth* by up to 95%; bandwidth demands are a large problem facing data parallel systems because the communication that must occur between the devices is proportional to the number of parameters.

Despite the many benefits of pipeline parallelism, existing techniques focus purely on the distributed setting [9, 7] and make hardware efficiency sacrifices to preserve synchronous execution (with the goal of preserving statistical efficiency, e.g. classification accuracy). *Synchronous execution* in this context means that the weights used for computation during forward propagation are the same as those used to compute the gradients during backward propagation (as if the entire gradient was computed in one step). Existing approaches preserve synchronous execution by trading off throughput (by adding bubbles into the pipeline, which underutilizes the hardware) and/or memory (by storing additional weight copies for microbatching). Importantly, these costs increase with the pipeline depth (as illustrated in Figure 1) even though the intention of increasing the pipeline depth is to improve the throughput. This poses a massive challenge for the type of fine-grained pipeline parallelism that one would want to run inside new hardware accelerators. Motivated by both new hardware accelerators and the distributed setting, in this paper we study how to remove these hardware overheads during pipeline parallel training by revisiting the fundamental question: *is purely synchronous execution necessary during neural network training?* Our contributions and outline are as follows.

- In Section 2, we introduce a model for *asynchronous* pipeline-parallel training, that, by eschewing synchronous execution, maximizes hardware efficiency by avoiding both pipeline bubbles and substantial memory increases.

- Using this model, in Section 3 we propose **PipeMare**, a system of three techniques that enables asynchronous pipeline training to maximize statistical efficiency. These techniques are: a *learning rate rescheduling* scheme, a *discrepancy correction*, and *warmup epochs*. For each technique, we motivate it theoretically by analyzing a quadratic objective, empirically extend it to deep learning, and empirically investigate its tradeoffs on both the hardware and statistical efficiency. We show that asynchronous pipeline-parallel training without these techniques typically results in divergence.

- In Section 4, we show that PipeMare can achieve competitive model accuracy with better hardware utilization compared to synchronous training (GPipe and PipeDream). On a ResNet50 model we show that we can match the synchronous baseline test accuracy (95%) on CIFAR10 and come within 0.9% of it (76.4%)

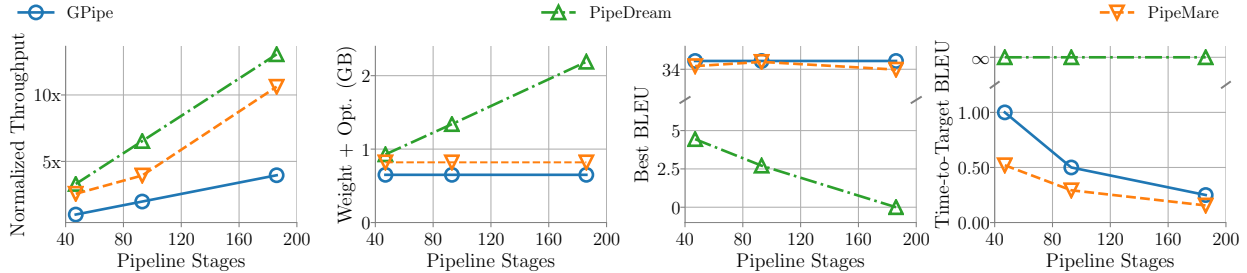


Figure 2: The impact of the number of pipeline stages on throughput, weight and optimizer memory, final model quality, and time-to-quality across different pipeline parallel training methods on a 12-layer Transformer model performing machine translation on the IWSLT14 dataset. Unlike PipeMare, GPipe and PipeDream suffer hardware costs (either throughput or the sum of weight and optimizer memory) proportional to the number of pipeline stages. Without these costs, PipeMare achieves a final model quality competitive with the best technique. Note that in our time-to-quality study, PipeDream is unable to achieve an acceptable final model quality, resulting in an infinite time-to-quality metric. For the clarity of demonstration, the throughput in the left most plot is normalized with respect to GPipe with 47 stages.

on ImageNet while running up to 3.3x faster and with up to 2.0x less weight and optimizer memory. On a Transformer model we show that PipeMare matches the BLEU score of synchronous baselines on both the IWSLT14 (34.5 BLEU score) and WMT17 tasks (27.8 BLEU score) while running up to 2.6x faster and with up to 1.9x less weight and optimizer memory than synchronous pipeline parallel training techniques.

## 1.1 Related Work

Our work extends previous pipeline-parallel training work (GPipe and PipeDream) as well as other (non-pipeline-parallel) asynchronous training techniques.

**PipeDream** PipeDream [7] is a pipeline parallel distributed training technique used primarily to reduce high computation to communication ratios. PipeDream showed up to 5x speedups in time-to-given accuracy metrics when compared to existing state-of-the-art data parallel training techniques. PipeDream is one type of memory hungry pipelining approach; their core technique is called weight stashing which maintains an additional copy of the weights for each minibatch flowing through the pipeline. This ensures synchronous computation with a fixed pipeline delay update. Our approach is similar to PipeDream except without weight stashing. This means we incur a similar pipeline delayed update to PipeDream but also that we run the forwards and backwards pass on different versions of the weights. PipeDream is one type of memory hungry pipelining approach; their core technique is called weight stashing which maintains an additional copy of the weights for each minibatch flowing through the pipeline.

**GPipe** GPipe [9] is a pipeline parallel distributed training technique originally deployed on TPUs [10]. GPipe is one type of throughput poor pipelining approach; the core technique used in GPipe is microbatching to hide the latency from introducing bubbles into the pipeline. This preserves synchronous execution. A consequence of this approach is that it also requires extra activation memory to preserve synchronous execution across batch boundaries. The authors use a gradient checkpointing technique [4] to alleviate this memory cost by recomputing activations at specified boundaries. Using these techniques, they show that pipeline parallelism can enable them to train larger models than ever on TPUs. In this paper, we focus on leveraging microbatching to reduce asynchrony but we also validate that, like GPipe, PipeMare can leverage the standard technique of gradient checkpointing to reduce activation memory (see Appendix A.1). Unlike GPipe, we focus on fine-grained parallelism with no bubbles in our pipeline.

**Hogwild!** Asynchronous training has been studied in several other contexts, the most well-known of which is Hogwild! [16]. In Hogwild! settings, as in pipeline-parallel settings, gradients are computed based on

delayed versions of weights. However, these delays are random and can vary from step to step and weight to weight, unlike the fixed pipeline delay that we have in the pipeline-parallel setting. In Appendix E we extend and apply PipeMare to this setting [15] showing that it can also improve final model accuracies here.

## 2 Preliminaries

We formally define a model of pipeline parallelism and asynchronous learning that forms the basis for the remainder of this paper. In Section 2.1 we define the model, and in Section 2.2 we analyze the delays, throughput, and weight memories of GPipe, PipeDream, and PipeMare; we show that PipeMare has higher throughput and lower weight memory usage than synchronous training techniques (GPipe and PipeDream) at the cost of higher asynchrony (or more delay). Our results are summarized in Figure 2 which shows that PipeMare’s final model quality is competitive despite the additional asynchrony.

### 2.1 Model

We now define our model for pipeline parallel DNN training and the asynchrony it can introduce (via two delay terms).

**Pipeline Parallelism** Pipeline-parallel training of a DNN works by decomposing the  $L$  layers (or operators) of the neural network into  $P$  pipeline stages, each of which is assigned to a parallel worker (this worker can range from a full distributed machine to a section of silicon on an accelerator). Layers optionally have weights associated with them; for this we let  $W$  represent the total size of all the weights in the model. While processing a minibatch of size  $B$ , each pipeline stage processes  $M$  samples at a time, where  $M$  is called the *microbatch size* and  $M \leq B$ . We use  $N$  to represent the number of microbatches in a minibatch (or  $N = \lceil \frac{B}{M} \rceil$ ). The resulting microbatch gradients are accumulated into gradient buffers, and weights are updated only at minibatch boundaries. Previous work studied the distributed case where  $P \ll L$ : we call this *coarse-grained pipeline parallelism*. Here, we are interested in the case of *fine-grained pipeline parallelism*, where  $P \approx L$ .

**Delay** The statistical effect of using pipeline-parallel training is characterized by the *pipeline delay*: the number of optimizer steps that pass between when the weights are read to compute a gradient and when that gradient is used to update the weights. In a standard backpropagation algorithm, each weight is read twice—once in the forward pass, and again in the backward pass—so there are *two* delay values,  $\tau_{\text{fwd}}$  and  $\tau_{\text{bkwd}}$ , which can vary by stage. Intuitively,  $\tau_{\text{fwd}}$  corresponds to the delay between a weight’s forward pass and it’s update. The earlier a pipeline stage the larger  $\tau_{\text{fwd}}$  value, i.e.,  $\tau_{\text{fwd},i} \propto (P - i)$  for the  $i$ th stage. Similarly,  $\tau_{\text{bkwd}}$  is the delay between a weight’s backward pass and it’s update. We can write this out formally as

$$w_{t+1} = w_t - \alpha \nabla f_t(u_{\text{fwd},t}, u_{\text{bkwd},t})$$

where  $w_t$  are the weight values after  $t$  gradient steps,  $\nabla f_t$  is the gradient function for the  $t$ -th minibatch, and  $u_{\text{fwd},t}$  and  $u_{\text{bkwd},t}$  are the (delayed) values of the weights that are used in the forward and backward passes, respectively, for computing  $\nabla f_t$ . More explicitly, the weights  $w_t$  can be broken up into weight vectors for each stage:  $(w_t)_1$  for stage 1,  $(w_t)_2$  for stage 2, et cetera, such that  $w_t = [(w_t)_1, (w_t)_2, \dots, (w_t)_P]$ . Concretely, the weight value  $(w_t)_i$  for stage  $i$  denotes the value of the weights for that stage after  $t$  gradient updates have been written to it (note that this means  $w_t$  as a whole is not necessarily the value of the weights in memory at any fixed stage-independent time  $t$ ), and the delayed weight values are defined for each pipeline stage  $i \in \{1, \dots, P\}$  as

$$(u_{\text{fwd},t})_i = (w_{t-\tau_{\text{fwd},i}})_i \quad \text{and} \quad (u_{\text{bkwd},t})_i = (w_{t-\tau_{\text{bkwd},i}})_i$$

where  $(\cdot)_i$  denotes selecting the weights for the  $i$ th stage. Notice that this is a bit of an abuse of notation—here, we are letting  $\nabla f_t(u_{\text{fwd},t}, u_{\text{bkwd},t})$  denote *the value of the gradient that would be computed* by the

	Forward delay $\tau_{\text{fwd}}$	Backward delay $\tau_{\text{bkwd}}$	Normalized throughput	Weights memory
PipeDream	$\frac{2(P-i)+1}{N}$	$\frac{2(P-i)+1}{N}$	1.0	$W \times \frac{P}{N}$
GPipe	0	0	$\frac{N}{N+P-1}$	$W$
PipeMare	$\frac{2(P-i)+1}{N}$	0	1.0	$W$

Table 1: Characterization of pipeline parallel training methods.  $\tau_{\text{fwd}}$  and  $\tau_{\text{bkwd}}$  are the pipeline delays for model weights in the forwards and backwards pass.  $W$  is one copy of the weights.  $P$  is the number of pipeline stages.  $N$  is the number of microbatches in a minibatch.  $i$  indexes the pipeline stage.

backpropagation algorithm using the weights  $u_{\text{fwd},t}$  in the forward pass and weights  $u_{\text{bkwd},t}$  in the backward pass. That is, the gradient  $\nabla f_t$  is a function of *two* weight vectors, rather than one (as is usual for SGD), because the pipeline-parallel model may use different values for the weights in the forward and backward pass. Synchronous execution corresponds to the case of  $u_{\text{fwd},t} = u_{\text{bkwd},t}$ , which requires setting  $\tau_{\text{fwd}} = \tau_{\text{bkwd}}$ : this reduces  $\nabla f_t$  to the ordinary case where it is a function of just a single weight vector. That is, if  $u_{\text{fwd},t} = u_{\text{bkwd},t}$

$$\nabla f_t(u_{\text{fwd},t}, u_{\text{bkwd},t}) = \nabla f_t(u_{\text{fwd},t}, u_{\text{fwd},t}) = \nabla f_t(u_{\text{fwd},t}), \quad (1)$$

where here the last term on the right has  $\nabla f_t$  denoting the ordinary mathematical gradient, which is a function of a single weight vector, while the other two terms have  $\nabla f_t$  denoting the value that would be computed by backpropagation using possibly different weights in the forward and backward passes. For the rest of this paper, we will use  $\nabla f_t$  with two arguments to denote this backpropagation-with-different-weights gradient, and use  $\nabla f_t$  with one argument to denote the ordinary mathematical gradient. Techniques to date have not shown how to train well when  $\tau_{\text{fwd}} - \tau_{\text{bkwd}} \neq 0$ .

## 2.2 Pipeline Parallel Training Methods

Using this setup we now analyze the delays, throughput, and memory usage of the two synchronous baseline pipeline parallel training methods (PipeDream and GPipe) and our asynchronous method (PipeMare). The results of this analysis are summarized in Table 1.

**PipeDream** PipeDream has forward delay  $\tau_{\text{fwd},i} = 2(P-i) + 1$  and uses weight stashing to cache the weights used in the forward pass until they are needed in the backward pass, which allows for full pipeline efficiency while maintaining synchronous execution  $\tau_{\text{fwd}} = \tau_{\text{bkwd}}$ . To accomplish this, each layer in our neural network has a fixed forward and backwards delay of  $\tau_{\text{fwd}} = \tau_{\text{bkwd}} = \frac{2(P-i)+1}{N}$  where  $i$  stands for the  $i$ th stage in the pipeline and  $N$  is the number of microbatches in a minibatch. Therefore for the first layer  $\tau_{\text{fwd}} = \tau_{\text{bkwd}} = \frac{2P-1}{N}$ . Note that because  $\tau_{\text{fwd}} = \tau_{\text{bkwd}}$  in PipeDream they run their forwards and backwards passes on the same copy of the weights, despite having a delayed update. Unfortunately, this comes at the cost of storing additional weight memory of size  $Mem = W \times \frac{P}{N}$ . With fine-grained pipeline parallelism  $P$  can become large (a problem for large models). As for throughput, because PipeDream’s pipeline is fully utilized without any bubbles during training they have a normalized throughput  $T = 1$ .

**GPipe** GPipe leverages microbatching to reduce the number of bubbles in its pipeline. For GPipe,  $\tau_{\text{fwd}} = \tau_{\text{bkwd}} = 0$ , at the cost of lower throughput and additional activation memory. Each pipeline has to be filled and drained at a minibatch boundary to ensure weight synchronization between forward and backward pass, so the average bubble time is  $O(\frac{P-1}{N+P-1})$  [9]. Consequently, the normalized (relative to PipeDream) throughput of GPipe is  $\frac{N}{N+P-1}$ . GPipe does not store any additional weight parameters but does store additional memory for activations. Using the standard technique of gradient checkpointing, both PipeMare and GPipe can reduce their activation memory footprint (see Appendix A.2).

**PipeMare** In PipeMare we let the computation proceed in an asynchronous fashion. Effectively, we are just computing gradients with whatever weights are in memory at the time we need to use them, which avoids

any need to store extra copies of our model weights ( $Mem = W$ ) or introduce bubbles into our pipeline ( $T = 1.0$ ), because as soon as a pipeline stage has its gradients (accumulated within a full minibatch) the weights are updated. This means that the forward propagation is done on different weights than those that are used for backpropagation, i.e.,  $\tau_{\text{fwd}} \neq \tau_{\text{bkwd}}$ . Concretely, each layer in our neural network has a fixed forward delay of  $\tau_{\text{fwd}} = \frac{2(P-i)+1}{N}$  which is the same  $\tau_{\text{fwd}}$  as PipeDream. On the other hand, since there is no delay between backward pass and weight updates,  $\tau_{\text{bkwd}} = 0$ . Similar to GPipe, minimizing the microbatch size  $M$  reduces the activation memory usage while also keeping each pipeline stage fully utilized. Unlike GPipe, minimizing the microbatch size in PipeMare has the additional benefit of helping to reduce asynchrony.

### 3 PipeMare

We design a strategy called **PipeMare** for asynchronous pipeline-parallel training of deep neural networks. PipeMare uses three techniques, which we introduce in this section. In Sections 3.1 to 3.3 we present each technique and empirically present its tradeoffs. In Sections 3.1 and 3.2 we provide a theoretical analysis to motivate the corresponding technique and delay the proof to Appendix B.

For our theoretical analysis, we examine what would happen if we used fixed-delay asynchronous gradient descent to optimize a one-dimensional convex quadratic. Even this very simple example has non-trivial behavior, and (as we will see) it exhibits many phenomena of interest seen in more complicated settings. Consider a one-dimensional quadratic objective  $f(w) = \frac{\lambda}{2}w^2$  for some fixed curvature  $\lambda > 0$ . Suppose that we run fixed-delay asynchronous SGD on this model, using gradient samples of the form

$$\nabla f_t(u_{\text{fwd},t}, u_{\text{bkwd},t}) = \lambda u_{\text{fwd},t} - \eta_t = \lambda w_{t-\tau} - \eta_t$$

where  $\eta_t$  is some gradient estimation noise, which we assume is bounded and depends on  $t$ . This implicitly assumes that the delays for all the weights are the same and equal to some fixed parameter  $\tau = \tau_{\text{fwd}}$ , with no delay discrepancy (we will consider delay discrepancy later in Section 3.2). Running SGD in this setting has the update step

$$\begin{aligned} w_{t+1} &= w_t - \alpha \nabla f_t(u_{\text{fwd},t}, u_{\text{bkwd},t}) \\ &= w_t - \alpha \lambda w_{t-\tau} + \alpha \eta_t. \end{aligned} \tag{2}$$

#### 3.1 Learning rate rescheduling (T1)

We theoretically derive our first technique—rescheduling the step size to be inversely proportional to the delay—and evaluate its tradeoffs on some DNN tasks.

**The problem.** We might hope that existing hyperparameters used for sequential SGD would “just work” for training in the asynchronous pipeline-parallel setting. Unfortunately, when we try running naively with a standard step size scheme, asynchronous pipeline-parallel SGD can significantly underperform the synchronous baseline. This happens because a large value of  $\tau$  can cause SGD to diverge even when using a step size  $\alpha$  for which the baseline synchronous algorithm converges. This is illustrated in Figure 3(a), which simulates the quadratic model (5) with  $\lambda = 1$ ,  $\alpha = 0.2$ , and  $\eta_t \sim \mathcal{N}(0, 1)$ , for various values of  $\tau$ . Notice that for  $\tau = 10$ , the trajectory diverges fairly quickly. In Appendix B.1, we show that the same phenomenon can be observed for a Resnet50 network.

**The theory.** The first question we want to ask is: *when will asynchronous pipeline-parallel SGD be stable on the quadratic model?* That is, for what values of the step size  $\alpha$  will it be guaranteed that  $w_t$  remains bounded, no matter what (bounded) noise signal  $\eta_t$  we get from the gradient estimator? To answer this question, notice that (2) is a linear system, which can be written in terms of a companion matrix that

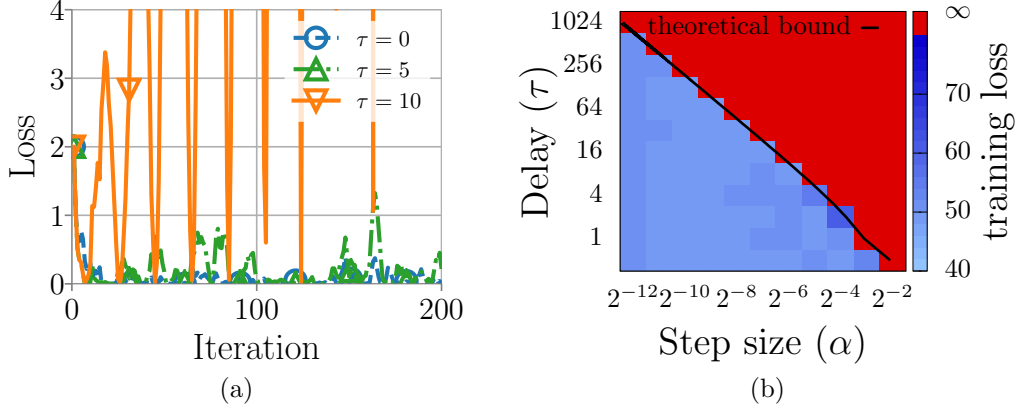


Figure 3: (a) Increasing  $\tau$  can cause the quadratic model to diverge even when  $\alpha$  remains fixed. (b) Evaluation of pipeline-parallel SGD for linear regression on the `cpusmall` dataset running for  $T = 10^6$  iterations. The heatmap reports losses as a function of the step size  $\alpha$  and the delay  $\tau$ ; red denotes divergence to  $\infty$ . The black curve shows the upper bound from Lemma 1 using the largest curvature of the objective in place of  $\lambda$ .

stores all the state of the system as

$$\begin{bmatrix} w_{t+1} \\ w_t \\ \vdots \\ w_{t-\tau+1} \end{bmatrix} = \begin{bmatrix} 1 & 0 & \cdots & 0 & -\alpha\lambda \\ 1 & 0 & \cdots & 0 & 0 \\ \vdots & \vdots & \ddots & \vdots & \vdots \\ 0 & 0 & \cdots & 1 & 0 \end{bmatrix} \begin{bmatrix} w_t \\ w_{t-1} \\ \vdots \\ w_{t-\tau} \end{bmatrix} + \begin{bmatrix} \alpha\eta_t \\ 0 \\ \vdots \\ 0 \end{bmatrix}.$$

If we call this  $(\tau + 1) \times (\tau + 1)$  companion matrix  $C$ , and call the vectorized version of  $w$  with its history  $W$ ,

$$W_{t+1} = CW_t + \alpha\eta_t e_1, \quad (3)$$

where  $e_1$  is the vector  $[1 \ 0 \ \cdots \ 0]^T$ . Linear systems of this type have solutions of the form

$$w_t = \sum_{k=0}^{t-1} \alpha\eta_{t-k-1} \sum_{\omega} \rho_{\omega}(k) \cdot \omega^k,$$

where the sum here ranges over the eigenvalues  $\omega$  of the companion matrix, and each  $\rho_{\omega}$  is a polynomial of degree less than the algebraic multiplicity of the eigenvalue  $\omega$ .<sup>1</sup> Thus, the convergence of (3) is determined entirely by  $C$ 's eigenvalues, and it will be stable if and only if all these eigenvalues lie inside the unit disk in the complex plane.  $C$ 's eigenvalues are the zeros of its characteristic polynomial

$$p(\omega) = \omega^{\tau+1} - \omega^{\tau} + \alpha\lambda. \quad (4)$$

So we want to find out for which values of  $\alpha$  the roots of  $p$  must all lie inside the unit disk.

**Lemma 1.** *The roots of the polynomial  $p$  of (4) all lie inside the unit disk if and only if the step size  $\alpha$  is set such that*

$$0 \leq \alpha \leq \frac{2}{\lambda} \cdot \sin\left(\frac{\pi}{4\tau + 2}\right) = O\left(\frac{1}{\lambda\tau}\right).$$

*Additionally, the roots are always isolated (of multiplicity 1), except at  $\alpha = \frac{1}{\lambda\tau} \left(\frac{\tau}{\tau-1}\right)^{\tau-1}$  where there is a root of multiplicity 2 at  $\omega = \frac{\tau}{\tau+1}$ .*

<sup>1</sup>To see why, consider the Jordan normal form of  $C$ , which will for each eigenvalue have a corresponding Jordan block of dimension equal to its algebraic multiplicity.

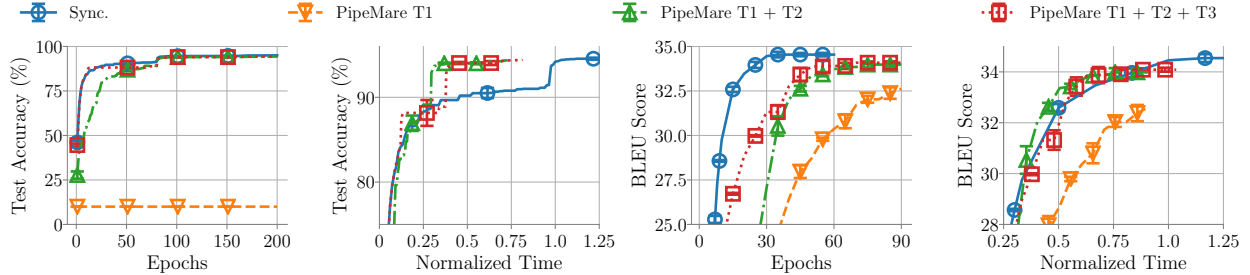


Figure 4: Effect of incrementally combining PipeMare techniques (T1, T2, and T3) on a ResNet50 (left two plots) and a 12-layer Transformer model (right two plots) with 214 and 186 pipeline stages respectively. This is 2x the number of pipeline stages when each model weight is treated at its own stage (as is done in Section 4). This tests the limits of our approach at an extreme (a fine-granularity of pipeline parallelism). Note in the plots, normalized time 1.0 represents the time synchronous training used to attain the targeted model accuracy.

This lemma gives us theoretical insight that backs up our empirical observations: when the delay is larger, the step size must be set smaller to prevent instability and divergence. It also gives us a way to quantify how much smaller we need to set the step size, predicting that  $\alpha = O(\tau^{-1})$ . In Figure 3(b) we validate that our theory not only applies to 1D optimization problems, but also can accurately describe what happens when we run pipeline-parallel SGD on a simple 12-dimensional linear regression problem using the cpusmall dataset [2]; the algorithm diverges at precisely an  $\alpha \propto \tau^{-1}$  slope, exactly what Lemma 1 predicts. In Appendix B.3 we extend this theory to SGD with momentum showing that the  $O(\tau^{-1})$  threshold is general and motivating our use of Technique 1 with *other learning algorithms such as Adam*, not just SGD.

**The technique.** We just showed that pipeline-parallel SGD (both with and without momentum) needs a step size that is inversely proportional to the delay: otherwise, it may become unstable and diverge. For deep learning, this motivates a choice of learning rate that is also inversely proportional to the delay. The natural choice here is to just divide the step size at each layer  $i$  by its delay  $\tau_i$ . However, this is (1) problematic because it leads to very small step sizes which slow convergence, and (2) unnecessary because it divides the step size by  $\tau$  even for later epochs where the base step size has already become small. While the inversely-proportional-to-delay step size makes sense for fixed-step-size learning, it is not necessarily the best choice when the step size is decreasing over time, as is usually done in deep learning [8, 19]. This motivates us to develop a step size scheme that (1) behaves like the  $O(\tau^{-1})$  scheme for early epochs when the learning rate is large, and (2) degrades back to the baseline learning rate scheme for later epochs with smaller step sizes.

**T1:** Suppose that we are training a DNN. In SGD step  $k$ , assign the following step size to layer  $i$ .

$$\alpha_{k,i} = \frac{\alpha_{k,base}}{\tau_i^{p_k}} \quad \text{where} \quad p_k = 1 - \min\left(\frac{k}{K}, 1\right). \quad (5)$$

where  $K$  is a hyperparameter representing a number of steps during which to adjust the learning rate, and  $\alpha_{k,base}$  denotes the normal synchronous learning rate. Empirically,  $K$  should increase with the fixed delay  $\tau_{fwd}$ . Here we suggest  $K$  to be one-quarter the number of steps spent in the first phase of a fixed step learning rate schedule (we use this for the ResNet model) or 5 times the linear warmup steps (minibatches) of a schedule with a linear warmup phase (we use this for the Transformer model).

**The tradeoffs.** As we just showed, learning rate rescheduling enables asynchronous pipeline-parallel training to converge in many cases that it otherwise would not. This technique comes with no hardware sacrifices (no extra memory or sacrifices in throughput). Unfortunately, as shown in Figure 4 this technique alone is not enough to ensure competitive final model qualities when a very fine granularity of pipeline parallelism is considered. This motivates our next two techniques which improve the final model qualities at the cost of minimal hardware sacrifices.



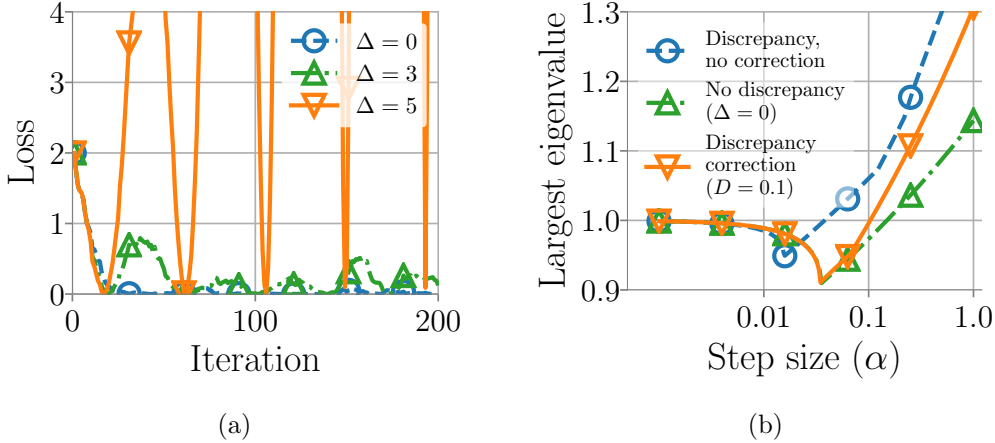


Figure 5: (a) Increasing  $\Delta$ , the gradient sensitivity to delay discrepancy, can cause the quadratic model to diverge even when  $\alpha$  and  $\tau$  remain fixed, using  $\tau_{\text{fwd}} = 10$ ,  $\tau_{\text{bkwd}} = 6$ , and  $\lambda = 1$ . (b) Effect of discrepancy correction on the quadratic model. Forward-backward delay discrepancy (blue) increases the largest magnitude eigenvalue of the companion matrix with  $\Delta = 5$ , and  $\tau$ ,  $\lambda$  same as in (a). Discrepancy correction with  $D = 0.1$  (orange) reduces the largest magnitude eigenvalue; this eigenvalue is closer to that attained without delay discrepancy (green).

### 3.2 Discrepancy correction (T2)

In Section 3.1, we analyzed a setting in which there was no delay discrepancy ( $\tau_{\text{fwd}} = \tau_{\text{bkwd}}$ ). In this subsection, we try to understand the effect of delay discrepancy, again using our quadratic model. We then develop and evaluate a technique for “correcting” this discrepancy.

**The problem.** To model delay discrepancy, we now assume gradient samples of the form

$$\nabla f_t(u_{\text{fwd},t}, u_{\text{bkwd},t}) = (\lambda + \Delta) \cdot w_{t-\tau_{\text{fwd}}} - \Delta \cdot w_{t-\tau_{\text{bkwd}}} - \eta_t$$

where  $\tau_{\text{fwd}} > \tau_{\text{bkwd}}$  are two different delays, and  $\Delta$  is a constant that measures the sensitivity of the gradients to discrepancy. We can think of this as the natural first-order (linear) approximation of  $\nabla f_t$  in the neighborhood of a stationary point—it models any affine function of  $u_{\text{fwd},t}$  and  $u_{\text{bkwd},t}$  that is consistent with the curvature  $\lambda$  when  $u_{\text{fwd},t} = u_{\text{bkwd},t}$ . More explicitly, it models any affine function that satisfies (1); that is, for any  $u$ ,

$$\nabla f_t(u, u) = \nabla f_t(u) = \lambda w - \eta_t.$$

If  $\Delta = 0$ , we recover a model of our original zero-discrepancy setting, whereas for large-magnitude values of  $\Delta$ , even a small delay discrepancy could be amplified to have a large effect on the gradient samples.

Delay discrepancy is problematic because it can amplify the divergence effect observed in Section 3.1. This is shown in Figure 5(a), which shows on the quadratic model (with  $\tau_{\text{fwd}} = 10$ ,  $\tau_{\text{bkwd}} = 6$ ,  $\lambda = 1$ , and  $\eta_t \sim \mathcal{N}(0, 1)$ ) that a nonzero value of  $\Delta$  can cause divergence even for a value of  $\alpha$  and  $\tau$  where with  $\Delta = 0$  (i.e. running PipeDream-style with no discrepancy) the trajectory would converge. In Appendix B.1, we illustrate that, just as was the case for the divergence phenomenon of Section 3.1, on ResNet50 asynchronous SGD with a large enough  $\Delta$  will diverge even for values of  $\alpha$  and  $\tau$  for which PipeDream-style SGD converged. We seek to understand this phenomenon theoretically and to develop a technique to limit its effect.

**The theory.** With our new discrepancy-dependent samples, pipeline-parallel SGD on our quadratic model has the update step

$$w_{t+1} = w_t - \alpha(\lambda + \Delta)w_{t-\tau_{\text{fwd}}} + \alpha\Delta w_{t-\tau_{\text{bkwd}}} + \alpha\eta_t,$$

which will have characteristic polynomial

$$p(\omega) = \omega^{\tau_{\text{fwd}}} \cdot (\omega - 1) - \alpha \cdot \Delta \cdot \omega^{\tau_{\text{fwd}} - \tau_{\text{bkwd}}} + \alpha \cdot (\lambda + \Delta). \quad (6)$$

As before, we can analyze this for stability by finding the value of  $\alpha$  for which the roots lie inside the unit disk.

**Lemma 2.** *For any  $\Delta > 0$ , there exists an  $\alpha > 0$  with*

$$\alpha \leq \min \left( \frac{2}{\Delta \cdot (\tau_{\text{fwd}} - \tau_{\text{bkwd}})}, \frac{2}{\lambda} \cdot \sin \left( \frac{\pi}{4\tau_{\text{fwd}} + 2} \right) \right)$$

*such that at least one of the roots of the polynomial  $p$  in (6) is outside the interior of the unit disk.*

This lemma shows two important things: first, that the maximal stable step size is still inversely proportional to the delay, even in the case where we can have forward-backward delay discrepancy; second, that for large values of  $\Delta$ , which indicate substantial deviation from the baseline case in which the delay discrepancy has no effect on the gradient, the largest stable  $\alpha$  becomes smaller (although still inversely proportional to  $\tau$ ). This models the behavior illustrated in Figure 5(a) where adding delay discrepancy exacerbates the divergence phenomenon.

**The technique.** As we have observed, delay discrepancy between the forward and backward passes can exacerbate the problem of divergence. If we could just compute  $\nabla f_t(u_{\text{fwd},t}, u_{\text{fwd},t})$  directly, then this mismatch would not be a problem. Unfortunately, in our asynchronous pipeline-parallel setting we cannot compute this, as we no longer have  $u_{\text{fwd},t}$  in memory by the time the backward pass comes around (since we have updated it between the forward and backward passes). To keep  $u_{\text{fwd},t}$  stored in memory between the forward and backward passes is possible, but undesirable as it would greatly increase the memory requirements of the algorithm (since multiple copies of the weights would need to be stored, as in PipeDream). Instead, we consider the question: is it possible to decrease the gap between  $u_{\text{fwd},t}$  and  $u_{\text{bkwd},t}$  by *approximating*  $u_{\text{fwd},t}$  without storing the full history of model weight values after  $u_{\text{fwd},t}$ ? By using a bit of extra memory to hold an approximation of the velocity of the weights, we can do this.

**T2:** *Instead of the assignment of  $u_{\text{bkwd}}$  from Section 3.1, set*

$$(u_{\text{bkwd},t})_i = (w_{t-\tau_{\text{bkwd}},i})_i - (\tau_{\text{fwd},i} - \tau_{\text{bkwd},i}) \delta_{t,i},$$

*where  $\delta_{t,i}$  is a newly added accumulator that estimates the amount that  $w_i$  is changing over time. It is kept up to date by the update step*

$$\delta_{t+1,i} = \gamma_i \cdot \delta_{t,i} + (1 - \gamma_i) \cdot (w_{t+1,i} - w_{t,i}),$$

*where  $\gamma_i$  is a decay rate parameter, assigned per-stage to  $\gamma_i = D^{1/(\tau_{\text{fwd},i} - \tau_{\text{bkwd},i})}$ , where  $D$  is a tunable global hyperparameter, determining the length of averaged history.*

Essentially, this technique adjusts the value of the weights used in the backward pass by extrapolating what the weights were during the forward pass based on the recent average trajectory of the weights. Applying T2 on the quadratic model also results in an update step that can be modeled with a companion matrix; we analyzed this system—just as before—by considering that companion matrix’s eigenvalues. This yielded two insights.

First, as the delay  $\tau_{\text{fwd}}$  increases, we can show that the points  $\omega$  at which an eigenvalue first crosses the unit circle as the step size  $\alpha$  increases from 0 approach  $\omega = 1$ . To build intuition about this large- $\tau$  regime, we examined the Taylor’s series of its characteristic polynomial at  $\omega = 1$ . Interestingly, if we set  $\gamma$  such that  $\gamma = 1 - 2/(\tau_{\text{fwd}} - \tau_{\text{bkwd}} + 1)$ , the second-order Taylor expansion of the  $p$  around  $\omega = 1$  is independent of  $\Delta$ . That is, we completely removed the impact of the gradients’ sensitivity to delay discrepancy (which is what  $\Delta$  measures), at least locally in the neighborhood of  $\omega = 1$ . For large  $\tau$ , this choice of  $\gamma$  is asymptotically equivalent to setting  $D = \exp(-2) = 0.135$ , so we generally choose to set  $D$  somewhere around here.

Second, using T2 seems to usually increase the allowable range of  $\alpha$  for which the quadratic model is stable. This effect is illustrated in Figure 5(b). In order to get a sense of whether we can expect T2 to be useful on a particular instance, we can evaluate this threshold of stability numerically in a quadratic model we believe to be representative, comparing the companion matrices both with and without correction. In the appendix, we do this exhaustively for values of the delay ranging up to 50, and observe across all evaluated cases with  $\Delta > 0$  (as well as some cases where  $\Delta < 0$ ) that using the correction T2 (with  $\gamma$  assigned as above) allows for larger  $\alpha$  to be used.

**The tradeoffs.** Since it requires an extra memory buffer to store  $\delta_t$ , T2 is not free: however, this increase in memory is small relative to the cost of storing the entire history of  $w$ . Figure 4 shows that combining T1+T2 enables fine-grained pipeline parallelism to converge with ResNet50 on CIFAR10 when T1 alone cannot, which justifies the benefits in statistical performance brought by its 25%-33% weight and optimizer memory increase.<sup>2</sup>

### 3.3 Warmup epochs (T3)

We propose augmenting our training method by adding synchronous warmup epochs (making it a hybrid approach) to close the final model quality gaps shown in Figure 4. This forms the basis of our third and final technique.

**The problem.** While we have developed two useful heuristics based on our quadratic model, quadratics are an imperfect proxy for what happens in DNN training. This is particularly true in earlier epochs of training, because during later epochs we typically imagine that we are approaching some local minimum with an approximately quadratic local neighborhood. Earlier epochs do not behave in this way. This is reflected in our empirical results: on the IWSLT14 dataset, T1 and T2 alone are not enough to match the synchronous baseline method quality. We hypothesize that this occurs because the algorithm is initialized in a “bad region” of space that has high curvature, large gradient noise, or behaves otherwise in a way for which the quadratic model is a bad proxy (such highly non-convex regions have been observed in previous work [12]). That is, we hypothesize that there may be some regions of state space which the pipeline-parallel SGD algorithm is bad at escaping, relative to the standard SGD algorithm. To correct for this, we propose a third technique, which can be used when T1 and T2 are insufficient.

**T3** *When training, initialize with  $M$  epochs of synchronous (GPipe-style) pipeline-parallel SGD using the standard learning rate. Afterwards, switch to asynchronous pipeline-parallel SGD. Empirically, we discovered that  $M = 10$  was more than sufficient to enable effective learning on both classification and translation tasks.*

**The tradeoffs.** This technique captures the intuition that since we know that baseline SGD does a good job of escaping these “bad regions” of initialization, we can use it to escape the “bad regions” (if any) before running pipeline-parallel SGD. However, this comes at a cost, since it requires running some more expensive non-pipeline-parallel epochs for initialization: Technique 3 presents a tradeoff between hardware efficiency and statistical efficiency. In Figure 4 we show that the impact of T3 when measuring time-to-given-accuracy is minimal and enables us to achieve noticeable statistical improvements with the Transformer model on the IWSLT14 dataset.

## 4 Experiments

We evaluate PipeMare on two standard image recognition tasks and neural machine translation tasks. Our evaluation supports the following two main claims:

- *PipeMare enables more efficient end-to-end training.* We show that across two image recognition and two neural machine translation tasks, PipeMare can attain up to  $3.3\times$  speedup in time-to-accuracy over the synchronous GPipe; we also show that PipeMare can attain a final model quality that PipeDream cannot reach, while using up to  $2\times$  less weight and optimizer memory.
- *PipeMare achieves final model qualities similar to those attained by synchronous training.* We show that PipeMare can achieve a final model accuracy within 0.9% of synchronous baselines on image recognition tasks and match the BLEU score of synchronous baselines on neural machine translation tasks. Through an ablation study, we show that this is only possible when PipeMare leverages all three techniques presented in Section 3.

---

<sup>2</sup>The discrepancy correction needs to store the velocity of the weight updates in addition to the model weight, the gradient and the momentum term in SGD optimizer; the total memory used by the SGD optimizer is thus increased by 33%. Similarly when using Adam optimizer, the increase is 25% because Adam stores both first and second order moments.

Table 2: Comparison on statistical efficiency, throughput and time-to-accuracy attained by PipeMare and baselines. Here we use top-1 accuracy (BLEU score) as the metrics for CIFAR10 and ImageNet (IWSLT and WMT). The target accuracy (BLEU score) is 1.0% (0.4) worse than the best accuracy (BLEU score) we can achieve with all three methods. The asynchronous methods (PipeDream and PipeMare) have higher throughputs, while the synchronous approach (GPipe) attains better statistical efficiency, i.e., requiring less epochs to targeted accuracy. When comparing the final time-to-accuracy, PipeMare can outperform both GPipe and PipeDream. ‘-’ indicates that the method was unable to reach the target metric.

Dataset	Method	Best metric	Target metric	Speedup to Target	Epochs to Target	Throughput	Weight+optimizer Memory
CIFAR10	PipeDream	94.8		<b>3.3X</b>	<b>82</b>	<b>1.0X</b>	2.70X
	GPipe	<b>95.0</b>	94.0	1.0X	83	0.3X	<b>1.0X</b> (270MB)
	PipeMare	<b>95.0</b>		<b>3.3X</b>	<b>82</b>	<b>1.0X</b>	1.33X
ImageNet	PipeDream	74.7		-	-	<b>1.0X</b>	1.61X
	GPipe	<b>76.4</b>	75.4	1.0X	<b>70</b>	0.3X	<b>1.0X</b> (293MB)
	PipeMare	75.5		<b>2.5X</b>	94	<b>1.0X</b>	1.33X
IWSLT14	PipeDream	0.0		-	-	<b>1.0X</b>	2.06X
	GPipe	<b>34.5</b>	34.1	1.0X	<b>30</b>	0.3X	<b>1.0X</b> (0.65GB)
	PipeMare	<b>34.5</b>		<b>1.7X</b>	35	0.6X	1.25X
WMT17	PipeDream	0.0		-	-	<b>1.0X</b>	2.39X
	GPipe	27.5	27.4	1.0X	<b>50</b>	0.3X	<b>1.0X</b> (1.01GB)
	PipeMare	<b>27.8</b>		<b>2.6X</b>	54	0.9X	1.25X

## 4.1 Experimental Setting

We provide an overview of our experimental setup and refer the reader to Appendix C for the exact details.

**Setup** We benchmark a ResNet50 model [8] for image classification and the 12-layer Transformer model [19] to benchmark neural machine translation because each represents standard benchmarks in their respective domains [1]. We use the standard CIFAR10 and ImageNet datasets for image classification, and popular IWSLT14 German-to-English and WMT17 English-to-German dataset for neural machine translation. For image classification, we use test set accuracy as the model accuracy metric while in translation tasks we use test BLEU score. We compare PipeMare to two synchronous (baseline) pipeline parallel training methods: GPipe and PipeDream. We report in detail on the two non-standard hyperparameters we had to select next (microbatch size and number of pipeline stages). For all other hyperparameters we use standard, publicly available hyperparameters (see Appendix C.1) for each of these two popular models.

**Microbatch Size** For microbatch size we always select a value that is as small as possible. This has two main benefits: (1) it saves activation memory proportional to the size of a microbatch and (2) it results in less gradient delay  $\tau_{fwd}$  given a fixed number of pipeline stages (more microbatches per minibatch). In more detail, we choose a microbatch size of 8 for ResNet50 on CIFAR10 and a microbatch size of 16 for ResNet50 on ImageNet as smaller microbatches in both cases can cause issues for batch normalization [24] layers. For Transformer on IWSLT14 we choose the maximum tokens per microbatch to be 245 because this is the number of tokens in the longest sentence present in IWSLT14 (and therefore is the smallest size we can select without losing information within a sentence). For Transformer on WMT17, we choose a maximum tokens per microbatch of 1792 to speed up experimental time (see Appendix C.4).

**Pipeline Stages** To partition the model into pipeline stages during training, we traverse model weights according to their topological order in the computation graph, always treating the weight and bias in the same layer as a single model weight (i.e. always in the same pipeline stage). Next, we divide these model weights evenly into P stages to split model weights across pipeline stages. This represents a very fine granularity of

Table 3: Ablation study of PipeMare. We show the impact of the learning rate rescheduling (T1), discrepancy correction (T2), and warmup epochs (T3) on metrics of interest. Note that warmup epochs were not necessary on the CIFAR10 dataset to recover the performance attained by GPipe. ‘-’ indicates that the method was unable to reach the target metric.

Dataset	Method	Best metric	Target metric	Speedup to Target	Epochs to Target	Throughput	Weight+optimizer Memory
CIFAR10	T1 Only	<b>95.0</b>		<b>3.3X</b>	83	<b>1.0X</b>	<b>1.0X</b> (270MB)
	T2 Only	94.5	94.0	3.2X	86	<b>1.0X</b>	1.33X
	T1+T2	<b>95.0</b>		<b>3.3X</b>	<b>82</b>	<b>1.0X</b>	1.33X
IWSLT14	T1 Only	34.1		1.6X	60	<b>1.0X</b>	<b>1.0X</b> (0.65GB)
	T2 Only	0.0		-	-	<b>1.0X</b>	1.25X
	T1 + T2 Only	34.1	34.1	1.6X	60	<b>1.0X</b>	1.25X
	T1 + T2 + T3	<b>34.5</b>		<b>1.7X</b>	<b>35</b>	0.6X	1.25X

pipeline parallelism which is a difficult one to train. Specifically, with ResNet50 we use 107 stages and with 12-layer Transformer we use 91 or 93 stages<sup>3</sup>; these are the largest number of stages with at least one model weight assigned to each pipeline stage.

**Metrics** We report time-to-accuracy, throughput, model weight and optimizer memory, and best accuracy (or BLEU score) on each benchmark. For the time-to-accuracy comparison, we use a target model accuracy metric value which is 1.0% (0.4) worse than the best test accuracy (BLEU score) attained via all three methods.<sup>4</sup> The execution throughput is estimated using the throughput model in Section 2. Using this and the number of epochs we compute an estimated time-to-target-quality metric. To report model weight and optimizer memory, we include both the master weights and all the copies required by the optimizer. For PipeDream, we additionally sum all the stashed weights (proportional to  $\tau_{\text{fwd}}$ ) of each stage. We report the averaged model accuracy from runs with three different random seeds and the time-to-accuracy speedup is measured over the averaged model accuracy.

## 4.2 End-to-End Comparison

We compare the asynchronous PipeMare training method to the synchronous GPipe and PipeDream methods on both image classification and machine translation tasks. In Table 2 we show that on both of these tasks PipeMare achieves faster time-to-accuracy while achieving comparable final model qualities—the greatest difference being a 0.9% top-1 accuracy difference on ImageNet.

**Image classification tasks** As shown in Table 2, on both the CIFAR10 and ImageNet dataset, PipeMare can respectively achieve  $3.3\times$  and  $2.5\times$  speedups over GPipe in terms of time-to-accuracy. More concretely, on CIFAR10 PipeMare attains the target accuracy using one less epoch than GPipe while GPipe demonstrates lower throughput than PipeMare; this results in our  $3.3\times$  speed up in time-to-accuracy. Note for the CIFAR10 and ImageNet experiment, PipeMare attains a full pipeline throughput of 1.0 because we do not need any warmup epochs here. This observation further indicates the efficacy of our techniques to speedup time-to-accuracy by improving the statistical efficiency. Though PipeDream attains the same throughput and same time-to-accuracy as PipeMare, it can require  $2.0\times$  more weight and optimizer memory (see Table 2).

**Neural machine translation tasks** As demonstrated in Table 2, PipeMare can achieve  $1.7\times$  and  $2.6\times$  speedup over GPipe on the IWSLT14 and WMT17 dataset. When comparing the PipeMare to the

<sup>3</sup>Transformer model for WMT17 employs shared embedding between encoder, decoder and projection while IWSLT14 has independent embeddings.

<sup>4</sup>For BLEU score, we select the threshold 0.4 to ensure we can perform ablation studies on IWSLT14. The best BLEU scores attained by PipeMare matches the best BLEU scores of synchronous pipeline parallel training baselines.

PipeDream approach, we can further observe PipeDream fails to train Transformer even though it uses  $1.9\times$  more weight and optimizer memory than PipeMare. On the other hand GPipe trains the model fine but sacrifices either throughput or activation memory to maintain its statistical efficiency. Because we use T3 (warmup epochs) on both the IWSLT14 (10 warmup epochs) and WMT17 (4 warmup epoch) experiments respectively the amortized throughput of PipeMare is smaller than 1. Still, by combining all three techniques we show that we improve the time-to-accuracy because T3 improves the statistical efficiency (at the cost of a worse throughput).

### 4.3 Ablation study

To understand the contribution of each technique to the performance of PipeMare, we perform ablation studies on PipeMare with respect to time-to-accuracy. We show that (1) the learning rate rescheduling technique plays an important role in the time-to-accuracy performance, (2) the discrepancy correction technique can accelerate time-to-accuracy when combined with learning rate rescheduling and (3) the warmup epoch technique can further trade-off hardware efficiency for better statistical efficiency to attain higher model accuracy and better time-to-accuracy. We show that each technique is necessary for PipeMare to outperform synchronous techniques from both a hardware and statistical efficiency perspective.

**Learning rate rescheduling (T1)** The asynchronous pipeline parallel training method with only learning rate rescheduling fully utilizes the compute power by avoiding both bubbles in the execution pipeline and additional weight memory. Therefore it achieves optimal hardware efficiency when compared to any other approach. In Table 3 we show that this alone can achieve a test accuracy of 95.0% and a test BLEU score of 34.1, both of which are competitive to the baseline 95.0% accuracy and 34.5 BLEU score of synchronous methods. In terms of time-to-accuracy, learning rate rescheduling alone achieves  $3.3\times$  and  $1.6\times$  speedup over GPipe—indicating its important role in improving statistical efficiency as well as time-to-accuracy. For ResNet50 on CIFAR10, the test accuracy of asynchronous training with learning rate rescheduling matches that of synchronous training while asynchronous training without it diverges—emphasizing the importance of T1 during synchronous training. For the Transformer model, T1 takes about twice as many epochs of synchronous training to reach BLEU score 34.1 while asynchronous training without T1 achieves a test BLEU score  $\leq 1$ .

**Discrepancy Correction (T2)** As shown in table 3, discrepancy correction in isolation achieves a test accuracy of 94.5% for ResNet 50 and a jarring 0.0 test BLEU score on the Transformer model. The poor Transformer model training is fixed by combining discrepancy correction with learning rate rescheduling, though the final BLEU score achieved is the same as in the learning rate scheduling only setting (34.1). Discrepancy correction with learning rate rescheduling shines on the ResNet50 model on CIFAR10 where the final test accuracy is 95.0%, a 0.5% improvement over only using learning rate rescheduling. This of course comes at the cost of using more weight memory. We find this cost to be minimal ( $0.25 - 0.33\times$  more) when compared to the speedups for time-to-a-given-accuracy ( $1.6\times$  faster than GPipe) and the final model quality improvements found while using this technique in conjunction with learning rate rescheduling. To further validate the efficacy of discrepancy correction, in Appendix C.2.2, we show that on a ResNet 152 model with 150 stages discrepancy correction is necessary to prevent divergence and match the model accuracy attained by synchronous training.

**Warmup Epochs (T3)** As shown in Table 3 learning rate rescheduling and discrepancy correction leave a noticeable BLUE score gap (0.4) for the Transformer model running on the IWSLT14 dataset. To close this gap PipeMare adds 10 synchronous (GPipe-style) warmup epochs on top of learning rate rescheduling and discrepancy correction. Indeed, as shown in table 3, the best BLEU score attained by asynchronous training is boosted from 34.1 to 34.5 and the time-to-accuracy speedup is boosted from  $1.6\times$  to  $1.7\times$ . Unfortunately this comes at the cost of decreasing the throughput from  $1.0\times$  to  $0.6\times$ . Conversely, for ResNet50 on CIFAR10 we find that warmup epochs did not improve our statistical metrics. As such we present our results here without T3. As indicated by these results, the number of warmup epochs can be treated as an additional hyperparameter for balancing hardware efficiency and statistical efficiency. To avoid the need to exhaustively tuning this hyperparameter, as a general rule of thumb we found that 10 synchronous warmup epochs was

more than sufficient to ensure optimal PipeMare training results. We refer to Appendix C.2.1 for more time-to-accuracy comparisons with different numbers of warmup epochs.

## 5 Conclusion

In this paper, we presented PipeMare, a system for asynchronous pipeline-parallel training of DNN models. PipeMare uses a bubble-free pipeline-parallel hardware model along with three theoretically motivated techniques (learning rate rescheduling, discrepancy correction, and warmup epochs) which help improve statistical efficiency. Experimentally, we showed PipeMare often has better time-to-accuracy than competing algorithms. We hope that this will make PipeMare a promising candidate algorithm for use with the new generation of hardware chips designed for training DNNs.

## References

- [1] Fair and useful benchmarks for measuring training and inference performance of ml hardware, software, and services. 2019. URL <https://mlperf.org/>.
- [2] Chih-Chung Chang and Chih-Jen Lin. LIBSVM: A library for support vector machines. *ACM Transactions on Intelligent Systems and Technology*, 2:27:1–27:27, 2011. Software available at <http://www.csie.ntu.edu.tw/~cjlin/libsvm>.
- [3] Tianqi Chen, Bing Xu, Chiyuan Zhang, and Carlos Guestrin. Training deep nets with sublinear memory cost. *arXiv preprint arXiv:1604.06174*, 2016.
- [4] Tianqi Chen, Bing Xu, Chiyuan Zhang, and Carlos Guestrin. Training deep nets with sublinear memory cost. *CoRR*, abs/1604.06174, 2016. URL <http://arxiv.org/abs/1604.06174>.
- [5] Christopher M De Sa, Ce Zhang, Kunle Olukotun, and Christopher Ré. Taming the wild: A unified analysis of hogwild-style algorithms. In *Advances in neural information processing systems*, pages 2674–2682, 2015.
- [6] Andrew Feldman. Cerebras wafer scale engine: An introduction. 2019. URL <https://www.cerebras.net/wp-content/uploads/2019/08/Cerebras-Wafer-Scale-Engine-Whitepaper.pdf>.
- [7] Aaron Harlap, Deepak Narayanan, Amar Phanishayee, Vivek Seshadri, Nikhil Devanur, Greg Ganger, and Phil Gibbons. PipeDream: Fast and efficient pipeline parallel DNN training. *arXiv preprint arXiv:1806.03377*, 2018.
- [8] Kaiming He, Xiangyu Zhang, Shaoqing Ren, and Jian Sun. Deep residual learning for image recognition. In *Proceedings of the IEEE conference on computer vision and pattern recognition*, pages 770–778, 2016.
- [9] Yanping Huang, Yonglong Cheng, Dehao Chen, HyoukJoong Lee, Jiquan Ngiam, Quoc V Le, and Zhifeng Chen. Gpipe: Efficient training of giant neural networks using pipeline parallelism. *arXiv preprint arXiv:1811.06965*, 2018.
- [10] Norman P Jouppi, Cliff Young, Nishant Patil, David Patterson, Gaurav Agrawal, Raminder Bajwa, Sarah Bates, Suresh Bhatia, Nan Boden, Al Borchers, et al. In-datacenter performance analysis of a tensor processing unit. In *2017 ACM/IEEE 44th Annual International Symposium on Computer Architecture (ISCA)*, pages 1–12. IEEE, 2017.
- [11] Thorsten Kurth, Jian Zhang, Nadathur Satish, Evan Racah, Ioannis Mitliagkas, Md Mostofa Ali Patwary, Tareq Malas, Narayanan Sundaram, Wahid Bhimji, Mikhail Smorkalov, et al. Deep learning at 15pf: supervised and semi-supervised classification for scientific data. In *Proceedings of the International Conference for High Performance Computing, Networking, Storage and Analysis*, page 7. ACM, 2017.

- [12] Hao Li, Zheng Xu, Gavin Taylor, Christoph Studer, and Tom Goldstein. Visualizing the loss landscape of neural nets. In *Advances in Neural Information Processing Systems*, pages 6389–6399, 2018.
- [13] Yinhan Liu, Myle Ott, Naman Goyal, Jingfei Du, Mandar Joshi, Danqi Chen, Omer Levy, Mike Lewis, Luke Zettlemoyer, and Veselin Stoyanov. Roberta: A robustly optimized BERT pretraining approach. *CoRR*, abs/1907.11692, 2019. URL <http://arxiv.org/abs/1907.11692>.
- [14] Ioannis Mitliagkas, Ce Zhang, Stefan Hadjis, and Christopher Ré. Asynchrony begets momentum, with an application to deep learning. In *2016 54th Annual Allerton Conference on Communication, Control, and Computing (Allerton)*, pages 997–1004. IEEE, 2016.
- [15] Benjamin Recht, Christopher Re, Stephen Wright, and Feng Niu. Hogwild: A lock-free approach to parallelizing stochastic gradient descent. In *Advances in neural information processing systems*, pages 693–701, 2011.
- [16] Benjamin Recht, Christopher Ré, Stephen J. Wright, and Feng Niu. Hogwild: A lock-free approach to parallelizing stochastic gradient descent. In *Advances in Neural Information Processing Systems 24: 25th Annual Conference on Neural Information Processing Systems 2011. Proceedings of a meeting held 12-14 December 2011, Granada, Spain.*, pages 693–701, 2011. URL <http://papers.nips.cc/paper/4390-hogwild-a-lock-free-approach-to-parallelizing-stochastic-gradient-descent>.
- [17] Ilya Sutskever, James Martens, George Dahl, and Geoffrey Hinton. On the importance of initialization and momentum in deep learning. In *International conference on machine learning*, pages 1139–1147, 2013.
- [18] Christian Szegedy, Sergey Ioffe, and Vincent Vanhoucke. Inception-v4, inception-resnet and the impact of residual connections on learning. *CoRR*, abs/1602.07261, 2016. URL <http://arxiv.org/abs/1602.07261>.
- [19] Ashish Vaswani, Noam Shazeer, Niki Parmar, Jakob Uszkoreit, Llion Jones, Aidan N Gomez, Lukasz Kaiser, and Illia Polosukhin. Attention is all you need. In *Advances in neural information processing systems*, pages 5998–6008, 2017.
- [20] Sally Ward-Foxton. Graphcore ceo touts ‘most complex processor’ ever. *EE Times*, 2019. URL <https://www.eetimes.com>.
- [21] Sally Ward-Foxton. Habana debuts record-breaking ai training chip. *EE Times*, 2019. URL <https://www.eetimes.com>.
- [22] Ashia C Wilson, Rebecca Roelofs, Mitchell Stern, Nati Srebro, and Benjamin Recht. The marginal value of adaptive gradient methods in machine learning. In *Advances in Neural Information Processing Systems*, pages 4148–4158, 2017.
- [23] Zhilin Yang, Zihang Dai, Yiming Yang, Jaime G. Carbonell, Ruslan Salakhutdinov, and Quoc V. Le. Xlnet: Generalized autoregressive pretraining for language understanding. *CoRR*, abs/1906.08237, 2019. URL <http://arxiv.org/abs/1906.08237>.
- [24] Kaiming He Yuxin Wu. Group normalization. *arXiv preprint arXiv:1803.08494*, 2018.



## A Supplementary material for Section 2

To better explain the hardware efficiency of the pipeline parallel training methods introduced in Section 2.2, we discuss the memory footprint and the throughput of the introduced methods in more details. In Appendix A.1, we first discuss the activation memory which is the major component of memory consumption in pipeline-parallel training. We then propose a new gradient checkpointing method to trade moderate compute for significantly lower activation memory footprint in Appendix A.2, which is applicable to both the synchronous and asynchronous methods introduced in Section 2.2. Finally, we discuss the throughput of the synchronous (GPipe) and asynchronous (PipeDream and PipeMare) methods under the same budget for activation memory and compute (measured in FLOPs), which is used to estimate the time-to-accuracy across the paper.

To discuss with consistent notations across methods, we define  $M$  and  $N$  respectively as the activation size per microbatch per neural net layer and the number of microbatches in each minibatch. We assume that we use models with  $L$  layers, which are trained using a pipeline with  $P$  stages. For clarity and simplicity in exposing the memory footprint and throughput, we assume that the model layers are partitioned equally across stages and the activation memory usage of each layer is the same.

### A.1 Activation Memory

**PipeMare and PipeDream** PipeMare and PipeDream has the same amount of activation memory requirement. This is because in both scenarios, pipeline does not have bubbles or stalls; the activations are cached and utilized with the same pipeline behavior pattern. In particular, the activation memory cached by stage  $i$  is proportional to the number of stages between forward and backward, i.e.,  $O(2(P - i) + 1)$ . Therefore, the total activation memory is

$$A_{PM} = O(MPL). \quad (7)$$

**GPipe** Here we discuss on the activation memory consumption of GPipe [9]. When the activations of every layer in neural nets are cached for backpropagation, by multiplying the activation memory per minibatch per layer  $B = MN$  with the number of layers  $L$ , we have the activation memory for GPipe as

$$A_{GP} = O(MNL). \quad (8)$$

When re-materialization proposed by [9] is considered, we only need to store the activations of a minibatch at every stage boundary, and recompute the activations for all the layers inside the stage. Therefore the activation memory per stage is  $O(MN + M\frac{L}{P})$ , with the total activation memory reduced to:

$$\tilde{A}_{GP} = O(MNP + ML) = O(M(NP + L)).$$

When  $P \ll L$ , the saving on activation memory is significant. However, in the fine-grain pipeline-parallel setting when  $P \approx L$ , the above equation goes back to eq. (8) and demonstrates negligible memory savings. This observation motivates us to propose the PipeMare recompute technique in Appendix A.2, which can apply to both synchronous (GPipe) and asynchronous (PipeMare) and effectively reduce the activation memory in fine-grained pipeline training.

### A.2 Trade compute for memory via PipeMare Recompute

In the fine-grain pipeline training setting, we have  $P \approx L$ . For simplicity in discussion, we assume  $P = L$ . In this setting, eq. (7) becomes,

$$A_{PM} = O(MP^2). \quad (9)$$

In other words, while throughput increases linearly with number of stages  $P$ , activation memory can scale quadratically. In order to reduce the memory pressure, here we propose a new way of utilizing recompute,

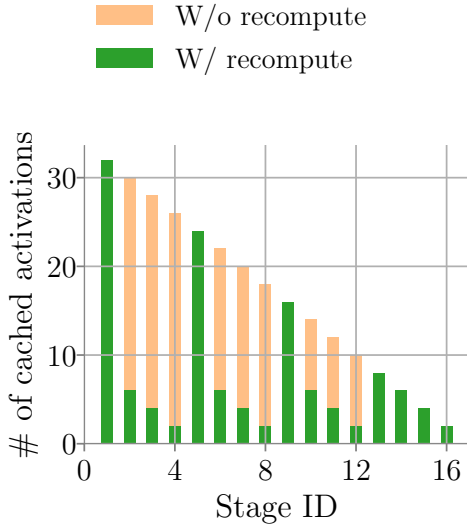


Figure 6: Activation memory footprint of PipeMare recompute in each pipeline stage. In this plot, we demonstrate the # of activations at each stage using an example with 16 stages equally split into 4 segments. The green bars in the plot stands for the memory consumption of each stage in terms of the number of microbatch activations copies in PipeMare with PipeMare recompute. The orange bars stands for the additional memory required when recompute is not used.

to trade a small amount of compute resources for huge activation memory savings. Instead of recomputing the activations inside each stage [9], we propose to recompute the activations across a segment of multiple stages, which we call PipeMare Recompute, to allow effective activation memory reduction in the fine-grain pipeline setting.

PipeMare Recompute utilizes a simple strategy. It recomputes the activation in advance so that the recomputed activation of the last stage in a segment arrives right at the time when the corresponding backpropagation needs to process this activation. Unlike the single-stage recompute proposed in GPipe [9], PipeMare Recompute does not stall the backpropagation operations as it can be overlapped with the forward and backward operations in the same pipeline stage. In order to enable this overlap, we need to consume approximately 25% of the total compute resources. Specifically, the pipeline needs to simultaneously compute for the forward, backward and recompute operations, with the backward operations consuming  $2\times$  more compute than forward and recompute operations respectively.

For the simplicity of demonstrating the activation memory saving attained by PipeMare Recompute, we assume  $P = L$  in the fine-grain pipeline setting and group the stages into segments each with  $S$  stages. Let us assume the  $i$ -th stage is the beginning stage of a specific segment, then the memory consumption for this segment is  $O(2(P - i) + S^2)$ . As visualized in Figure 6 for an example with 16 stages and 4 segments, the first term  $2(P - i)$  in the segment-wise activation memory is for caching activations at the first stage in the segment for recompute. The second term  $S^2$  then describes the memory buffers needed for recomputed activations that are used by backward pass (e.g., recompute of  $j$ -th stage in a segment needs to start  $2(S - j)$  steps earlier before the corresponding gradient arrives at this stage). Consequently, given the memory consumption in each segment is  $O(2(P - i) + S^2)$ , the total memory with  $P/S$  segments is determined by

$$A_{PM}^r(S) = O\left(M(P + S^2) \cdot \frac{P}{S}\right) = O\left(MP\left(\frac{P}{S} + S\right)\right).$$

When  $S = \sqrt{P}$ , we can get the minimum memory consumption,

Mode	w/o PipeMare Recompute	w/ PipeMare Recompute
GPipe	$MPN$	$MPN^{\frac{1}{2}}$
PipeMare/PipeDream	$MP^2$	$MP^{\frac{3}{2}}$

Table 4: Activation memory requirement by GPipe, PipeDream and PipeMare. Here we assume the total number of pipeline stages is the same as total neural network layers/operators, i.e.,  $P = L$ . Note the activation memories for PipeMare and PipeDream are the same.

Dataset	number of stages	Activation memory without recompute	Activation memory with recompute
CIFAR10	107		<b>0.097X</b>
ImageNet	107	1X	<b>0.097X</b>
IWSLT14	93		<b>0.104X</b>
WMT17	91		<b>0.105X</b>

Table 5: Activation memory of PipeMare for various tasks. Activation memory can be significantly reduced by using PipeMare Recompute.

$$A_{PM}^r = O\left(MP^{\frac{3}{2}}\right). \quad (10)$$

Note the quadratic dependency on  $P$  in Equation (9) is reduced to a power of  $\frac{3}{2}$ , indicating a significantly lowered activation memory in the fine-grain pipeline-parallelism with large  $P$  values.

We can similarly apply the PipeMare recompute technique to GPipe as well. In order to overlap recompute with forward and backward pass, each stage (except the first stage) in a segment needs to cache the same amount of activations as those of PipeMare. Whereas for the first stage in each segment, it needs to cache  $N$  instead of  $2(P - i)$  activations. This is because GPipe stalls at the boundary of minibatch, and there are  $N$  microbatches to be processed in the minibatch. That being said, the activation memory of GPipe is  $O(M(N + S^2) \cdot \frac{P}{S})$ . Thus when  $S = \sqrt{N}$ , the minimum activation memory footprint of GPipe is

$$A_{GP}^r = O\left(MPN^{\frac{1}{2}}\right). \quad (11)$$

We summarize the activation memory consumption with and without recompute for GPipe, PipeDream and PipeMare in Table 4. We can observe that for both synchronous and asynchronous pipeline-parallel training, the PipeMare Recompute can significantly reduce the activation memory in the fine-grain pipeline parallelism with large number of stages. The concrete activation memory saving of PipeMare on various tasks discussed in main text is shown in table 5.

### A.3 The throughput of GPipe and PipeMare

In Section 4, we present the time-to-accuracy comparison between GPipe and PipeMare. In this section, we analyze the relative throughput of GPipe with respect to PipeMare. We show that under the same budget for activation memory and compute resource (FLOPs), by wisely selecting the microbatch size in GPipe, the optimal configuration of GPipe can only achieve approximately  $0.3\times$  throughput of PipeMare (and PipeDream) using the same number of pipeline stages.

For the clarity of discuss, we first consider the situation without recompute. We consider a latency model where the latency of an operator is constant before the compute resource is not fully utilized, while the latency increases linearly with the microbatch size after the utilization of compute resource saturates.<sup>5</sup> For PipeMare, we assume the budget for both activation memory and compute resource are saturated with the same microbatch size  $M_{PM}$ . For the simplicity of discussion, we assume the latency of a PipeMare stage

<sup>5</sup>This model describes the behavior of matrix multiply operations on typical hardware such as GPU.

is 1 (unit omitted) when processing a single microbatch of size  $M_{PM}$ . In PipeMare execution, the pipeline never stalls. Thus  $1/3$  of the compute resources are dedicated to forward operations while  $2/3$  are allocated to backward pass. In GPipe, it needs microbatch size  $3M_{PM}$  and  $3/2M_{PM}$  respectively to saturate the same compute resource budget in the forward and backward execution phase. Given the latency model described above, the latency of each Gpipe stage to process a single microbatch during forward is 1 when the microbatch size  $M_{GP}$  is smaller than  $3M_{PM}$  (compute resource underutilized) and  $\frac{M_{GP}}{3M_{PM}}$  when microbatch size is larger than  $3M_{PM}$  (compute resource utilization saturates). Applying the same reasoning for backward pass, we can derive that for each stage to process one microbatch in GPipe, the latency for forward and backward operations are

$$l_{fwd} = \max\left(\frac{M_{GP}}{3M_{PM}}, 1\right), l_{bwd} = \max\left(\frac{2M_{GP}}{3M_{PM}}, 1\right).$$

To fairly compare the throughput of GPipe and PipeMare, we optimize the throughput of GPipe by properly setting the microbatch size  $M_{GP}$ . Assume  $M_{GP} = \alpha M_{PM}$ , we have  $N = \frac{1}{\alpha}P$  to saturate the same activation memory budget according to Equation (7) and Equation (8). We derive the optimal throughput of GPipe by discussing three following cases.

**Case 1.** when  $\alpha \geq 3$ , the compute resource are saturated during forward and backward in GPipe. Thus we have  $l_{fwd} = \frac{1}{3}\alpha, l_{bwd} = \frac{2}{3}\alpha$ , so the latency of processing a full minibatch through forward and backward is:

$$(l_{fwd} + l_{bwd})(N + P) = (\alpha + 1)P.$$

Therefore the minimum latency is  $4P$ , indicating a maximum throughput of 0.25.

**Case 2.** when  $\alpha \leq \frac{3}{2}$ , the compute resource is under utilized for both the forward and backward pass. In this case, we have  $L_{fwd} = 1, L_{bwd} = 1$ . Thus the latency of a full forward and backward pass is:

$$(l_{fwd} + l_{bwd})(N + P) = 2\left(1 + \frac{1}{\alpha}\right)P.$$

We can derive that the minimum latency is  $\frac{10}{3}P$ , leading to a maximum throughput of 0.3 in this case.

**Case 3.** when  $\frac{3}{2} < \alpha < 3$ , the compute resource is saturated for backward but not for forward operations. We have  $L_{fwd} = 1, L_{bwd} = \frac{2}{3}\alpha$ . Thus the latency of processing a single minibatch is

$$(l_{fwd} + l_{bwd})(N + P) = \left(1 + \frac{2}{3}\alpha\right)\left(1 + \frac{1}{\alpha}\right) = \left(\frac{5}{3} + \frac{1}{\alpha} + \frac{2}{3}\alpha\right)P.$$

In this case, the minimum latency is  $\left(\frac{5}{3} + 2\sqrt{\frac{2}{3}}\right)P$  when  $\alpha = \sqrt{\frac{3}{2}}$  which indicates a maximum throughput of 0.30.

To summarize, we can observe that under the same activation memory budget, the maximum relative throughput of GPipe with respect to PipeMare is 0.3, which is attained when  $M_{GP} = \sqrt{\frac{3}{2}}M_{PM}$ . We use this maximum throughput of 0.3 to estimate the time-to-accuracy for GPipe in Section 4.

For a complete discussion, we also present the relative throughput of GPipe with respect to PipeMare with recompute. When recompute is enabled in PipeMare,  $\frac{1}{4}$  of the compute resource is used for forward pass and recompute independently, while the rest  $\frac{1}{2}$  is used during backward pass. When we apply the same PipeMare recompute technique to GPipe, the forward and backward latencies of GPipe with recompute are

$$l_{fwd} = \max\left(\frac{M_{GP}}{4M_{PM}}, 1\right), l_{bwd} = \max\left(\frac{3M_{GP}}{4M_{PM}}, 1\right).$$

Using the similar analysis as in the setting without recompute, we can show that the minimum latency of GPipe is  $\left(\frac{7}{4} + \sqrt{3}\right)P$ , i.e. the maximum throughput is 0.29.

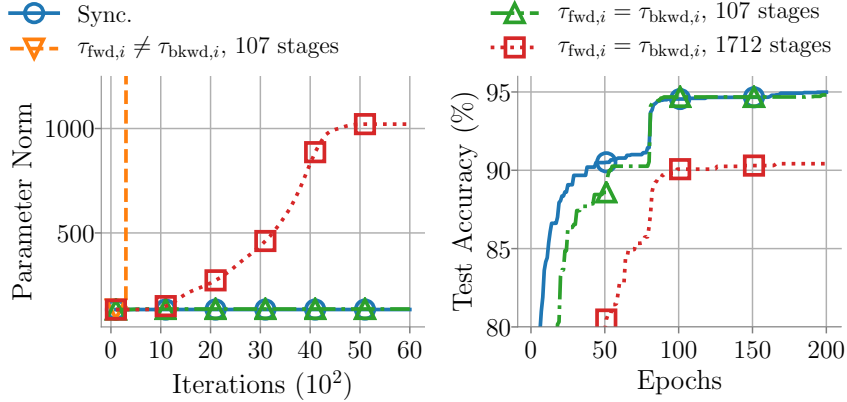


Figure 7: Analysis on the divergence for asynchronous pipeline-parallel training: the divergence is caused by the forward delay  $\tau_{\text{fwd},i}$ ; it is further exacerbated by forward-backward delay discrepancy when  $\tau_{\text{fwd},i} \neq \tau_{\text{bkwd},i}$ . Specifically in the left plot, we observe that using 428 stages without forward-backward delay discrepancy, asynchronous training diverges at the beginning. We also observe that with 107 stages, asynchronous training diverges with forward-backward delay discrepancy, while it does not diverge without forward-backward delay discrepancy; this indicates that delay discrepancy can exacerbate the divergence behavior. These observations motivates us to explore the technique to stabilize asynchronous pipeline-parallel training.

## B Supplementary material for Section 3

### B.1 Motivating examples in deep learning

Figure 7(a) illustrates that, just as we saw for the quadratic model, pipeline-parallel SGD can not be run naively with the same hyperparameters as would be used in the baseline model, since this would significantly negatively impact loss. Figure 7(b) shows why: pipeline-parallel SGD is *diverging* to infinity, completely failing to learn, even for a step size scheme for which the sequential model achieves state-of-the-art results. This matches our results on the quadratic model. For Resnet50 with standard hyperparameters, Figure 7 shows that this phenomenon is caused by the delay: the red series shows that, even when  $\tau_{\text{fwd},i} = \tau_{\text{bkwd},i}$  in simulation, substantially large fixed delay can cause the system to diverge. Figure 7 also illustrates that this divergence is exacerbated by forward-backward delay discrepancy: the orange series shows that even when the learning rate and delay  $\tau_{\text{fwd},i}$  are kept the same, adding delay discrepancy can cause the algorithm to diverge.

### B.2 Proof of Lemma 1

We start by trying to find the  $\alpha$  for which  $p$  has a complex root on the unit circle. Note that since  $(1 - iy)/(1 + iy)$  always lies on the unit circle for any  $y \in \mathbb{R}$ , it suffices to find  $\alpha$  for which

$$0 = p \left( \frac{1 - iy}{1 + iy} \right) = \left( \left( \frac{1 - iy}{1 + iy} \right) - 1 \right) \left( \frac{1 - iy}{1 + iy} \right)^\tau + \alpha \lambda.$$

for some  $y > 0$ . After a little simplification, this becomes

$$2iy \cdot (1 - iy)^\tau = \alpha \lambda \cdot (1 + iy)^{\tau+1}. \quad (12)$$

Next, we take the argument. Since  $y$ ,  $\alpha$ , and  $\lambda$  are real and positive, for some  $n \in \mathbb{Z}$ ,

$$\frac{\pi}{2} + 2\pi n + \tau \text{Arg}(1 - iy) = (\tau + 1) \text{Arg}(1 + iy),$$

which implies that, since  $\text{Arg}(1 - iy) = -\text{Arg}(1 + iy)$ ,

$$\text{Arg}(1 + iy) = \frac{\pi + 4\pi n}{4\tau + 2}.$$

This uniquely determines the value of  $y$ , because  $y = \tan \text{Arg}(1 + iy)$ . To get the corresponding value of  $\alpha$ , notice that if we take the magnitude of (12), it simplifies to

$$\alpha\lambda = \frac{|2iy|}{|1 + iy|} = \frac{2y}{\sqrt{1 + y^2}} = 2 \sin \text{Arg}(1 + iy),$$

so there can be a point on the unit circle when

$$\alpha = \frac{2}{\lambda} \cdot \sin\left(\frac{\pi + 4\pi n}{4\tau + 2}\right)$$

for any  $n \in \mathbb{Z}$ . The lemma statement now follows directly from a root-counting argument.

The main components of the root-counting argument are as follows. First, notice that for small  $\alpha$ , all the roots of  $p$  will be within the interior of the unit disk, since as  $\alpha$  approaches 0 from above, all but one of the roots will approach 0 and the remaining root will approach 1 from the left. To see this, notice that when  $\alpha = 0$ ,

$$p(\omega) = (\omega - 1) \cdot \omega^\tau.$$

On the other hand, as  $\alpha \rightarrow \infty$ , all the roots will diverge in magnitude to infinity, which means they must eventually leave the unit circle. To see why, notice that any root of  $p$  must satisfy

$$0 = p(\omega) = \omega^{\tau+1} - \omega^\tau + \alpha\lambda,$$

which implies from taking the magnitude that

$$|\omega|^{\tau+1} + |\omega|^\tau \geq \alpha\lambda.$$

Thus, we can conclude that all  $\tau + 1$  roots of the polynomial  $p$  must pass through the unit circle as  $\alpha$  moves from  $0_+$  to  $\infty$ .

Now, from the proof of Lemma 1, we know exactly where these crossings of the unit circle can occur. They happen for

$$\alpha = \frac{2}{\lambda} \cdot \sin\left(\frac{\pi + 4\pi n}{4\tau + 2}\right),$$

and at a point  $\omega$  on the unit circle with

$$\text{Arg}(\omega) = \pm \frac{\pi + 4\pi n}{4\tau + 2}.$$

Not all values of  $n$  correspond to a positive value of  $\alpha$ , and many values of  $n$  will result in the same value of  $\alpha$ . Clearly we can restrict our attention to  $0 \leq n < 2\tau + 1$ , since adding  $2\tau + 1$  to  $n$  results in the same values for  $\alpha$  and  $\omega$ . The step size  $\alpha$  will only be positive when, for some  $m \in \mathbb{Z}$ ,

$$\frac{\pi + 4\pi n}{4\tau + 2} + 2\pi m \in (0, \pi),$$

since this is where the sin is positive. Dividing both sides by  $\pi$  and multiplying by  $2\tau + 1$ , this happens when

$$\frac{1}{2} + 2n + 2m(2\tau + 1) \in (0, 2\tau + 1).$$

In other words, this will happen for  $n \in \{0, 1, \dots, \tau\}$ . However, half of these produce redundant values of  $\alpha$ , since

$$\begin{aligned} \sin\left(\frac{\pi + 4\pi(\tau - n)}{4\tau + 2}\right) &= \sin\left(\frac{\pi(4\tau + 2) - \pi - 4\pi n}{4\tau + 2}\right) \\ &= \sin\left(\pi - \frac{\pi + 4\pi n}{4\tau + 2}\right) \\ &= \sin\left(\frac{\pi + 4\pi n}{4\tau + 2}\right). \end{aligned}$$

So we can restrict our attention to  $0 \leq n \leq \frac{\tau}{2}$ . If  $\tau$  is odd, then each of these assignments of  $n$  corresponds to two roots on the unit circle. If  $\tau$  is even, then each of these assignments corresponds to two roots, except for the assignment  $n = \frac{\tau}{2}$ , for which

$$\text{Arg}(\omega) = \pm \frac{\pi + 2\pi\tau}{4\tau + 2} = \frac{\pi}{2}$$

corresponds to only one root on the unit circle. Thus there are only ever  $\tau + 1$  assignments of  $(\alpha, \omega)$  for which  $\omega$  is a root on the unit circle of

$$0 = (\omega - 1) \cdot \omega^\tau + \alpha\lambda.$$

Furthermore, none of those roots can be multiple roots, because if they were multiple roots they would need to be zeros of the polynomial  $p'(\omega)$ , and none of the roots of that polynomial lie on the unit disk. As a result, every root crossing of the unit disk must involve only a single root. Since there are  $\tau + 1$  roots and  $\tau + 1$  opportunities for a crossing, and all  $\tau + 1$  roots *must* cross at some point, each crossing of the unit circle must correspond to a root moving *out* of the unit disk. As a consequence, no root can ever move back in to the unit disk, since there is no room for it to do so. Thus, after the first roots leave the unit disk at

$$\alpha = \frac{2}{\lambda} \cdot \sin\left(\frac{\pi}{4\tau + 2}\right),$$

there is never a time at which all the roots are inside the unit disk.

Finally, recall that  $p$  can have a double root only where its first derivative  $p'$  has a root. This will occur only where

$$p'(w) = (\tau + 1)\omega^\tau - \tau\omega^{\tau-1} = 0,$$

which happens at

$$\omega = \frac{\tau}{\tau + 1}.$$

This corresponds to a value of  $\alpha$  of

$$\begin{aligned} \alpha &= \frac{1}{\lambda}(1 - \omega)\omega^\tau \\ &= \frac{1}{\lambda(\tau + 1)} \left(\frac{\tau}{\tau + 1}\right)^\tau. \end{aligned}$$

This proves the lemma.

### B.3 An extension to SGD with momentum.

Deep neural networks are often trained with momentum [17]. A natural question is whether the  $O(\tau^{-1})$  stability threshold also holds if momentum is used. When we add momentum, our update step becomes

$$v_{t+1} = \beta v_t - \alpha \nabla f_t(u_{\text{fwd},t}, u_{\text{bkwd},t}), \quad w_{t+1} = w_t + v_{t+1}.$$

We make the same simplifying assumptions as we made above for the non-momentum case, assuming a constant  $\tau$  and quadratic loss. This results in an update step that, just as above, can be expressed in terms of a companion matrix which will have characteristic polynomial

$$p(\omega) = \omega^{\tau+1} - (1 + \beta)\omega^\tau + \beta\omega^{\tau-1} + \alpha\lambda. \quad (13)$$

As in the non-momentum case, we can analyze this for stability by finding the parameters for which the roots of  $p$  lie inside the unit disk.

**Lemma 3.** *For any momentum parameter  $0 < \beta \leq 1$ , there exists a step size  $\alpha$  with*

$$0 < \alpha \leq \frac{4}{\lambda} \cdot \sin\left(\frac{\pi}{4\tau + 2}\right)$$

*such that at least one of the roots of the polynomial  $p$  of (14) lies outside the interior of the unit disk.*

This lemma shows that adding momentum does not let us escape from the  $O(\tau^{-1})$  step size requirement observed for SGD. It suggests that the  $O(\tau^{-1})$  threshold is general and not just specific to plain SGD, and it motivates our use of Technique 1 with *all learning algorithms*, not just SGD.

We make the same simplifying assumptions as we made above for the non-momentum case, assuming a constant  $\tau$  and quadratic loss. This results in an update step of

$$w_{t+1} - w_t = \beta(w_t - w_{t-1}) - \alpha\lambda w_{t-\tau} + \alpha\eta_t.$$

Just as in the non-momentum case, we can write this in terms of a companion matrix, which will have characteristic polynomial

$$p(\omega) = \omega^{\tau+1} - (1 + \beta)\omega^\tau + \beta\omega^{\tau-1} + \alpha\lambda. \quad (14)$$

As in the non-momentum case, we will analyze this for stability by finding the parameters for which the roots of  $p$  lie inside the unit disk.

To prove the lemma, we start with the expression for the polynomial

$$\begin{aligned} p(\omega) &= \omega^{\tau+1} - (1 + \beta)\omega^\tau + \beta\omega^{\tau-1} + \alpha\lambda \\ &= (\omega - \beta) \cdot (\omega - 1) \cdot \omega^{\tau-1} + \alpha\lambda. \end{aligned}$$

As for the non-momentum case, we consider the substitution

$$\omega = \frac{1 - iy}{1 + iy},$$

which always lies on the unit circle for any  $y \in \mathbb{R}$ . (Without loss of generality, we consider  $y > 0$ , which corresponds to roots in the lower half-plane. This is without loss of generality because, since  $p$  is a real polynomial, its complex roots always appear in pairs.) We want to find  $\alpha$  and  $\beta$  for which

$$\begin{aligned} 0 &= p\left(\frac{1 - iy}{1 + iy}\right) \\ &= \left(\left(\frac{1 - iy}{1 + iy}\right) - \beta\right) \left(\left(\frac{1 - iy}{1 + iy}\right) - 1\right) \left(\frac{1 - iy}{1 + iy}\right)^{\tau-1} \\ &\quad + \alpha\lambda. \end{aligned}$$

This can be simplified to

$$0 = \left(1 - \beta \cdot \frac{1 + iy}{1 - iy}\right) \left(\frac{-2iy}{1 + iy}\right) \left(\frac{1 - iy}{1 + iy}\right)^\tau + \alpha\lambda,$$



and so

$$\left(1 - \beta \cdot \frac{1 + iy}{1 - iy}\right) \cdot 2iy \cdot (1 - iy)^\tau = \alpha\lambda(1 + iy)^{\tau+1}.$$

Define  $\theta$  as

$$\theta = \text{Arg}\left(1 - \beta \cdot \frac{1 + iy}{1 - iy}\right) + \frac{\pi}{2}.$$

Notice that since the thing inside the Arg is 1 minus something with magnitude less than 1 times something that is on the unit circle in the upper half plane, it will necessarily end up in the fourth quadrant, and so

$$\theta - \frac{\pi}{2} \in \left(-\frac{\pi}{2}, 0\right) \Rightarrow \theta \in \left(0, \frac{\pi}{2}\right).$$

Now taking the argument of the whole expression gives us, for any  $n \in \mathbb{Z}$ ,

$$\theta + 2\pi n + \tau \text{Arg}(1 - iy) = (\tau + 1) \text{Arg}(1 + iy),$$

which simplifies to

$$\text{Arg}(1 + iy) = \frac{\theta + 2\pi n}{2\tau + 1}.$$

In this case,

$$y = \tan\left(\frac{\theta + 2\pi n}{2\tau + 1}\right).$$

Next, we derive an expression for  $\beta$ . Since

$$\begin{aligned} \theta &= \text{Arg}\left(1 - \beta \cdot \frac{1 + iy}{1 - iy}\right) + \frac{\pi}{2} \\ &= \text{Arg}\left(\frac{(1 - \beta) - iy(1 + \beta)}{1 - iy}\right) + \frac{\pi}{2} \\ &= \text{Arg}((1 - \beta) - iy(1 + \beta)) + \text{Arg}(1 + iy) + \frac{\pi}{2} \\ &= \text{Arg}\left(1 + i \frac{1 - \beta}{y(1 + \beta)}\right) + \text{Arg}(1 + iy), \end{aligned}$$

so

$$\theta - \frac{\theta + 2\pi n}{2\tau + 1} = \text{Arg}\left(1 + i \frac{1 - \beta}{y(1 + \beta)}\right),$$

and

$$\begin{aligned} \frac{1 - \beta}{1 + \beta} &= \tan\left(\frac{\theta + 2\pi n}{2\tau + 1}\right) \tan\left(\theta - \frac{\theta + 2\pi n}{2\tau + 1}\right) \\ &= \frac{\cos\left(\theta - \frac{2\theta + 4\pi n}{2\tau + 1}\right) - \cos(\theta)}{\cos\left(\theta - \frac{2\theta + 4\pi n}{2\tau + 1}\right) + \cos(\theta)}. \end{aligned}$$

Now taking the absolute value to find  $\alpha$  gives us

$$\begin{aligned} \alpha\lambda &= \left|1 - \beta \cdot \frac{1 + iy}{1 - iy}\right| \cdot \frac{2y}{|1 + iy|} \\ &= 2 \cdot \left|1 - \beta \cdot \frac{1 + iy}{1 - iy}\right| \cdot \sin\left(\frac{\theta + 2\pi n}{2\tau + 1}\right). \end{aligned}$$

Next, consider the case where  $n = 0$ . In this case,

$$\frac{1 - \beta}{1 + \beta} = \frac{\cos\left(\theta - \frac{2\theta}{2\tau+1}\right) - \cos(\theta)}{\cos\left(\theta - \frac{2\theta}{2\tau+1}\right) + \cos(\theta)}.$$

It is clear that there is a one-to-one relationship between accessible  $\theta$  and  $\beta$  here, because we can represent  $\beta = 0$  with  $\theta = \pi/2$ , and  $\beta = 1$  with  $\theta = 0$ . So, for every  $\beta$  (and given a fixed  $\tau$ ), we can find a  $\theta$  that satisfies this equation. Using that  $\theta$ , we can then assign

$$y = \tan\left(\frac{\theta}{2\tau+1}\right).$$

Since  $\theta$  is bounded,  $y$  is guaranteed to be in range. So, the equation

$$0 = p\left(\frac{1 - iy}{1 + iy}\right)$$

will be guaranteed to hold for some  $\alpha$ . This  $\alpha$  will be given by

$$\alpha\lambda = 2 \cdot \left|1 - \beta \cdot \frac{1 + iy}{1 - iy}\right| \cdot \sin\left(\frac{\theta}{2\tau+1}\right).$$

So, since  $\beta < 1$ , it follows that this  $\alpha$  will satisfy

$$\alpha \leq \frac{4}{\lambda} \cdot \sin\left(\frac{\theta}{2\tau+1}\right) \leq \frac{4}{\lambda} \cdot \sin\left(\frac{\pi}{4\tau+2}\right),$$

which is what we wanted to show. This proves that for any  $\beta$ , there exists a  $\alpha$  at least this large for which the algorithm is unstable.

## B.4 Proof of Lemma 2

We know, from our baseline analysis, that when

$$\alpha = \frac{2}{\lambda} \cdot \sin\left(\frac{\pi}{4\tau+2}\right)$$

and  $\Delta = 0$ , the polynomial  $p$  has a root at

$$\omega = \exp\left(\frac{i\pi}{2\tau_{\text{fwd}}+1}\right).$$

Consider values of  $\alpha$  and  $\Delta$  for which  $p$  would have a root at

$$\omega = \exp(i\theta)$$

for

$$\theta \in \left(0, \frac{\pi}{2\tau_{\text{fwd}}+1}\right].$$

In this case, we'd have

$$\begin{aligned} 0 &= \exp(i\tau_{\text{fwd}}\theta) \cdot (\omega - 1) \\ &\quad - \alpha \cdot \Delta \cdot \exp(i(\tau_{\text{fwd}} - \tau_{\text{bkwd}})\theta) \\ &\quad + \alpha \cdot (\lambda + \Delta), \end{aligned}$$

which is equivalent to

$$\begin{aligned}
0 &= \exp\left(i\frac{\tau_{\text{fwd}} + \tau_{\text{bkwd}}}{2}\theta\right) \cdot (\omega - 1) \\
&\quad - \alpha \cdot \Delta \cdot \exp\left(i\frac{\tau_{\text{fwd}} - \tau_{\text{bkwd}}}{2}\theta\right) \\
&\quad + \alpha \cdot (\lambda + \Delta) \cdot \exp\left(-i\frac{\tau_{\text{fwd}} - \tau_{\text{bkwd}}}{2}\theta\right).
\end{aligned}$$

If we take the real part of this, we get

$$\begin{aligned}
0 &= \cos\left(\frac{\tau_{\text{fwd}} + \tau_{\text{bkwd}} + 2}{2} \cdot \theta\right) \\
&\quad - \cos\left(\frac{\tau_{\text{fwd}} + \tau_{\text{bkwd}}}{2} \cdot \theta\right) \\
&\quad + \alpha\lambda \cos\left(\frac{\tau_{\text{fwd}} - \tau_{\text{bkwd}}}{2}\theta\right) \\
&= -2 \sin\left(\frac{\tau_{\text{fwd}} + \tau_{\text{bkwd}} + 1}{2} \cdot \theta\right) \cdot \sin\left(\frac{\theta}{2}\right) \\
&\quad + \alpha\lambda \cos\left(\frac{\tau_{\text{fwd}} - \tau_{\text{bkwd}}}{2}\theta\right),
\end{aligned}$$

so solving for  $\alpha$  gives us

$$\alpha = \frac{2 \sin\left(\frac{\tau_{\text{fwd}} + \tau_{\text{bkwd}} + 1}{2} \cdot \theta\right) \cdot \sin\left(\frac{\theta}{2}\right)}{\lambda \cos\left(\frac{\tau_{\text{fwd}} - \tau_{\text{bkwd}}}{2} \cdot \theta\right)}.$$

On the other hand, if we take the imaginary part instead of the real part, we get

$$\begin{aligned}
0 &= \sin\left(\frac{\tau_{\text{fwd}} + \tau_{\text{bkwd}} + 2}{2} \cdot \theta\right) \\
&\quad - \sin\left(\frac{\tau_{\text{fwd}} + \tau_{\text{bkwd}}}{2} \cdot \theta\right) \\
&\quad - \alpha(\lambda + 2\Delta) \sin\left(\frac{\tau_{\text{fwd}} - \tau_{\text{bkwd}}}{2}\theta\right) \\
&= 2 \cos\left(\frac{\tau_{\text{fwd}} + \tau_{\text{bkwd}} + 1}{2} \cdot \theta\right) \cdot \sin\left(\frac{\theta}{2}\right) \\
&\quad - \alpha(\lambda + 2\Delta) \sin\left(\frac{\tau_{\text{fwd}} - \tau_{\text{bkwd}}}{2}\theta\right) \\
&= 2 \cos\left(\frac{\tau_{\text{fwd}} + \tau_{\text{bkwd}} + 1}{2} \cdot \theta\right) \cdot \sin\left(\frac{\theta}{2}\right) \\
&\quad - (\lambda + 2\Delta) \sin\left(\frac{\tau_{\text{fwd}} - \tau_{\text{bkwd}}}{2}\theta\right) \\
&\quad \cdot \frac{2 \sin\left(\frac{\tau_{\text{fwd}} + \tau_{\text{bkwd}} + 1}{2} \cdot \theta\right) \cdot \sin\left(\frac{\theta}{2}\right)}{\lambda \cos\left(\frac{\tau_{\text{fwd}} - \tau_{\text{bkwd}}}{2}\theta\right)} \\
&= 1 - \left(1 + \frac{2\Delta}{\lambda}\right) \tan\left(\frac{\tau_{\text{fwd}} - \tau_{\text{bkwd}}}{2}\theta\right) \\
&\quad \cdot \tan\left(\frac{\tau_{\text{fwd}} + \tau_{\text{bkwd}} + 1}{2} \cdot \theta\right).
\end{aligned}$$

and so

$$\begin{aligned}
\frac{2\Delta}{\lambda} &= \cot\left(\frac{\tau_{\text{fwd}} - \tau_{\text{bkwd}}}{2} \cdot \theta\right) \\
&\quad \cdot \cot\left(\frac{\tau_{\text{fwd}} + \tau_{\text{bkwd}} + 1}{2} \cdot \theta\right) - 1 \\
&= \csc\left(\frac{\tau_{\text{fwd}} - \tau_{\text{bkwd}}}{2} \cdot \theta\right) \\
&\quad \cdot \csc\left(\frac{\tau_{\text{fwd}} + \tau_{\text{bkwd}} + 1}{2} \cdot \theta\right) \\
&\quad \cdot \cos\left(\frac{2\tau_{\text{fwd}} + 1}{2} \cdot \theta\right).
\end{aligned}$$

One thing we notice immediately from this expression is that it approaches infinity as  $\theta \rightarrow 0^+$ , goes to zero at

$$\theta = \frac{\pi}{2\tau_{\text{fwd}} + 1},$$

and is continuous and positive in between. This means that all non-negative values of  $\Delta$  are actually attained for some  $\theta$ , and there is a one-to-one mapping between  $\Delta$  and  $\theta$  in this interval. Furthermore, since  $\alpha$  approaches 0 monotonically as  $\theta$  approaches 0 over this interval, this means that there is no absolute lower bound on how small  $\alpha$  can get. So all we need is a bound on  $\alpha$  in terms of  $\Delta$ .

In the limit of small  $\theta$ ,

$$\frac{2\Delta}{\lambda} = \left(\frac{\tau_{\text{fwd}} - \tau_{\text{bkwd}}}{2} \cdot \theta\right)^{-1} \cdot \left(\frac{\tau_{\text{fwd}} + \tau_{\text{bkwd}} + 1}{2} \cdot \theta\right)^{-1}$$

and

$$\begin{aligned}
\alpha &= \frac{2\left(\frac{\tau_{\text{fwd}} + \tau_{\text{bkwd}} + 1}{2} \cdot \theta\right) \cdot \left(\frac{\theta}{2}\right)}{\lambda} \\
&= \frac{2\left(\frac{\tau_{\text{fwd}} + \tau_{\text{bkwd}} + 1}{2} \cdot \theta\right) \cdot \left(\frac{\theta}{2}\right)}{\lambda} \cdot \frac{\lambda}{2\Delta} \\
&\quad \cdot \left(\frac{\tau_{\text{fwd}} - \tau_{\text{bkwd}}}{2} \cdot \theta\right)^{-1} \cdot \left(\frac{\tau_{\text{fwd}} + \tau_{\text{bkwd}} + 1}{2} \cdot \theta\right)^{-1} \\
&= \frac{1}{\Delta \cdot (\tau_{\text{fwd}} - \tau_{\text{bkwd}})}.
\end{aligned}$$

Can we get a real bound that matches this?

$$\begin{aligned}
\frac{\lambda}{\Delta} &= 2 \sin\left(\frac{\tau_{\text{fwd}} - \tau_{\text{bkwd}}}{2} \cdot \theta\right) \\
&\quad \cdot \sin\left(\frac{\tau_{\text{fwd}} + \tau_{\text{bkwd}} + 1}{2} \cdot \theta\right) \\
&\quad \cdot \sec\left(\frac{2\tau_{\text{fwd}} + 1}{2} \cdot \theta\right) \\
&= \left(\cos\left(\frac{2\tau_{\text{bkwd}} + 1}{2} \cdot \theta\right) - \cos\left(\frac{2\tau_{\text{fwd}} + 1}{2} \cdot \theta\right)\right) \\
&\quad \cdot \sec\left(\frac{2\tau_{\text{fwd}} + 1}{2} \cdot \theta\right) \\
&= \frac{\cos\left(\frac{2\tau_{\text{bkwd}} + 1}{2} \cdot \theta\right)}{\cos\left(\frac{2\tau_{\text{fwd}} + 1}{2} \cdot \theta\right)} - 1,
\end{aligned}$$

so

$$1 + \frac{\lambda}{\Delta} = \frac{\cos\left(\frac{2\tau_{\text{bkwd}}+1}{2} \cdot \theta\right)}{\cos\left(\frac{2\tau_{\text{fwd}}+1}{2} \cdot \theta\right)}.$$

It can be shown that for any  $y < x < \frac{\pi}{2}$ ,

$$\frac{\cos(y)}{\cos(x)} \geq 1 + \frac{x^2 - y^2}{2}.$$

(To see why, observe that for any  $a \in [0, 1]$ , the third derivative of  $\cos(ax) \cdot \sec(x)$  is non-negative over  $x \in [0, \pi/2]$ .) So,

$$\frac{\lambda}{\Delta} \geq \frac{1}{2} \cdot \left( \left( \frac{2\tau_{\text{fwd}}+1}{2} \right)^2 - \left( \frac{2\tau_{\text{bkwd}}+1}{2} \right)^2 \right) \cdot \theta^2.$$

Similarly, we have

$$\begin{aligned} \alpha &= \frac{2}{\lambda} \cdot \sin\left(\frac{\theta}{2}\right) \\ &\quad \cdot \frac{(\lambda+\Delta) \cdot \sin\left(\frac{2\tau_{\text{fwd}}+1}{2} \cdot \theta\right) + \Delta \cdot \sin\left(\frac{2\tau_{\text{bkwd}}+1}{2} \cdot \theta\right)}{\lambda+2\Delta} \\ &\leq \frac{1}{\lambda} \cdot \frac{(\lambda+\Delta) \cdot \left(\frac{2\tau_{\text{fwd}}+1}{2}\right) + \Delta \cdot \left(\frac{2\tau_{\text{bkwd}}+1}{2}\right)}{\lambda+2\Delta} \cdot \theta^2 \\ &\leq \frac{2}{\Delta} \cdot \frac{(\lambda+\Delta) \cdot \left(\frac{2\tau_{\text{fwd}}+1}{2}\right) + \Delta \cdot \left(\frac{2\tau_{\text{bkwd}}+1}{2}\right)}{\lambda+2\Delta} \\ &\quad \cdot \left( \left( \frac{2\tau_{\text{fwd}}+1}{2} \right)^2 - \left( \frac{2\tau_{\text{bkwd}}+1}{2} \right)^2 \right)^{-1} \\ &\leq \frac{2}{\Delta} \cdot \left( \left( \frac{2\tau_{\text{fwd}}+1}{2} \right) + \left( \frac{2\tau_{\text{bkwd}}+1}{2} \right) \right) \\ &\quad \cdot \left( \left( \frac{2\tau_{\text{fwd}}+1}{2} \right)^2 - \left( \frac{2\tau_{\text{bkwd}}+1}{2} \right)^2 \right)^{-1} \\ &\leq \frac{2}{\Delta} \cdot \left( \left( \frac{2\tau_{\text{fwd}}+1}{2} \right) - \left( \frac{2\tau_{\text{bkwd}}+1}{2} \right) \right)^{-1} \\ &\leq \frac{2}{\Delta \cdot (\tau_{\text{fwd}} - \tau_{\text{bkwd}})}. \end{aligned}$$

And this is an actual guarantee. So, we've proven that for any  $\Delta \geq 0$ , there exists an  $\alpha$  with

$$0 < \alpha \leq \frac{2}{\Delta \cdot (\tau_{\text{fwd}} - \tau_{\text{bkwd}})}$$

such that the polynomial  $p$  has a root on the unit circle. The other part of the min in the lemma statement follows directly from our original bound and the monotonicity of  $\Delta$  and  $\alpha$  in terms of  $\theta$  over the interval we have been looking at.

## B.5 Justification for Claims in Section 3.2

In Section 3.2, we motivated our choice of  $\Delta$  by claiming that the second-order Taylor expansion of the characteristic polynomial of the companion matrix associated with momentum-corrected asynchronous pipeline-parallel SGD on the quadratic model around  $\omega = 1$  is invariant to the delay-discrepancy-sensitivity parameter  $\Delta$  if  $\gamma$  is set appropriately. Here, we justify that assertion, as well as the other assertions we made in that subsection. First, we want to show formally that  $\omega = 1$  is the “interesting” region. We do this with the following lemma.

**Lemma 4.** For any polynomial functions  $f$ ,  $g$ , and  $h$ , and any integer  $\tau$ , define the polynomial

$$p_\tau(\omega) = (\omega - 1) \cdot f(\omega) \cdot \omega^\tau - \alpha \cdot g(\omega) \cdot \omega^\tau - \alpha \cdot h(\omega),$$

and suppose that  $f$  does not vanish anywhere on the unit circle. For any  $\tau$ , let  $\alpha_{\text{thresh}}(\tau)$  be the smallest  $\alpha > 0$  for which  $p_\tau$  has a root on the unit circle, and let  $\omega_{\text{thresh}}(\tau)$  be one of the corresponding roots. Then, if

$$\lim_{\tau \rightarrow \infty} \alpha_{\text{thresh}}(\tau) = 0,$$

then

$$\lim_{\tau \rightarrow \infty} \omega_{\text{thresh}}(\tau) = 1.$$

*Proof.* Suppose that  $p_\tau(\omega) = 0$  for some  $\omega$  on the unit circle. Solving for  $\alpha$  gives

$$\begin{aligned} \alpha &= (\omega - 1) \cdot \frac{f(\omega) \cdot \omega^\tau}{g(\omega) \cdot \omega^\tau - h(\omega)} \\ &= |\omega - 1| \cdot \frac{|f(\omega)|}{|g(\omega) \cdot \omega^\tau - h(\omega)|} \\ &\geq |\omega - 1| \cdot \frac{|f(\omega)|}{|g(\omega)| + |h(\omega)|} \\ &\geq |\omega - 1| \cdot \frac{f_{\min}}{g_{\max} + h_{\max}}, \end{aligned}$$

where these min and max are taken over the unit circle. So, for some constant  $C > 0$  independent of  $\tau$ ,

$$|\omega - 1| \leq C \cdot \alpha$$

(we know such a  $C$  exists because  $f$  does not vanish on the unit circle). The lemma statement follows directly.  $\square$

This lemma shows in a very general sense that the points at which the roots of the characteristic polynomial first cross the unit circle as  $\alpha$  increases from 0 will approach  $\omega = 1$  as  $\tau$  approaches  $\infty$ . Since we know from observation that for the systems we are studying, the smallest  $\alpha$  at which the polynomial becomes unstable becomes smaller as  $\tau$  approaches  $\infty$ , it follows that as  $\tau \rightarrow \infty$ , the points  $\omega$  at which the system first becomes unstable must also approach  $\omega = 1$ . This formally justifies our notion of the area where the “action happens” for large  $\tau$ .

Now, we will prove that the characteristic polynomial of the companion matrix associated with momentum-corrected asynchronous pipeline-parallel SGD on the quadratic model around  $\omega = 1$  is invariant to the delay-discrepancy-sensitivity parameter  $\Delta$  if  $\gamma$  is set such that

$$\gamma = 1 - \frac{2}{\tau_{\text{fwd}} - \tau_{\text{bkwd}} + 1}.$$

Here, we justify that assertion. First, observe that the characteristic polynomial of the companion matrix is

$$\begin{aligned} p(\omega) &= (\omega - 1)(\omega - \gamma)\omega^{\tau_{\text{fwd}}} \\ &\quad + \alpha(\lambda + \Delta)(\omega - \gamma) \\ &\quad - \alpha\Delta\omega^{\tau_{\text{fwd}} - \tau_{\text{bkwd}}}(\omega - \gamma) \\ &\quad + \alpha\Delta\omega^{\tau_{\text{fwd}} - \tau_{\text{bkwd}}}(\tau_{\text{fwd}} - \tau_{\text{bkwd}})(1 - \gamma)(\omega - 1). \end{aligned}$$

This can be seen by constructing the companion matrix from the update rule directly.

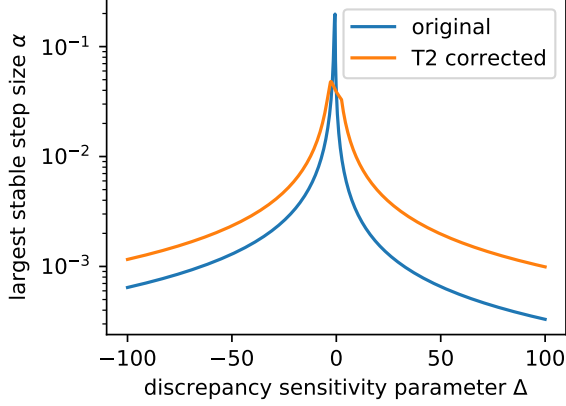


Figure 8: Plot of the largest step size  $\alpha$  for which all the eigenvalues of the companion matrix lie within the unit disk for various values of the discrepancy sensitivity parameter  $\Delta$ , comparing the original quadratic model with the T2 discrepancy-corrected model. This figure was generated for  $\tau_{\text{fwd}} = 40$  and  $\tau_{\text{bkwd}} = 10$ .

Notice that this polynomial satisfies all the conditions of the statement of Lemma 4, for appropriate values of  $f$ ,  $g$ , and  $h$ , and letting  $\tau = \tau_{\text{fwd}} - \tau_{\text{bkwd}}$ . At  $\omega = 1$ , we have

$$p(1) = \alpha\lambda(1 - \gamma)$$

and

$$p'(1) = \alpha\lambda + 1 - \gamma,$$

both of which are independent of the sensitivity parameter  $\Delta$ . On the other hand, the second derivative is

$$\begin{aligned} p''(1) &= 2\tau_{\text{fwd}}(1 - \gamma) + 2 \\ &\quad - \alpha\Delta(\tau_{\text{fwd}} - \tau_{\text{bkwd}})(1 + \gamma - (1 - \gamma)(\tau_{\text{fwd}} - \tau_{\text{bkwd}})). \end{aligned}$$

From here, notice that the  $\Delta$  term drops out of this expression if we set  $\gamma$  such that

$$0 = 1 + \gamma - (1 - \gamma)(\tau_{\text{fwd}} - \tau_{\text{bkwd}});$$

this occurs when

$$\gamma = 1 - \frac{2}{\tau_{\text{fwd}} - \tau_{\text{bkwd}} + 1}. \quad (15)$$

Also notice that in the limit of large  $\tau$ , we would have

$$\begin{aligned} D &= \gamma^{\tau_{\text{fwd}} - \tau_{\text{bkwd}}} \\ &= \left(1 - \frac{2}{\tau_{\text{fwd}} - \tau_{\text{bkwd}} + 1}\right)^{\tau_{\text{fwd}} - \tau_{\text{bkwd}}} \\ &\approx \exp(-2). \end{aligned}$$

This motivates our use of  $D$  nearby 0.135.

In Section 3.2, we also claimed that using T2 with the assignment in (15) seems to increase the allowable range over which the system is stable. In experiments on the quadratic model, we observed that this happens consistently for all values of  $\Delta > 0$  and for all  $\tau_{\text{fwd}}$  and  $\tau_{\text{bkwd}}$  we tried. We tried all values of  $\tau_{\text{fwd}} > \tau_{\text{bkwd}}$  where  $\tau_{\text{fwd}} \leq 40$  and values of  $\Delta$  ranging from  $-100$  to  $100$ ; this range of  $\tau$  covers the entire range of delays present in our DNN training experiments. While the improvement seems to happen always for  $\Delta \geq 0$ , if  $\Delta < 0$  we have observed (again only in numerical experiments) that T2 does not necessarily improve the threshold of stability for all values of  $\Delta$ . This is illustrated in Figure 8, which shows what happens for the particular case of  $\tau_{\text{fwd}} = 40$  and  $\tau_{\text{bkwd}} = 10$ . This figure is generally representative of what happens the cases we tried: the T2 correction makes the range of stable  $\alpha$  consistently bigger when  $\Delta \geq 0$ , while occasionally having a negative effect when  $\Delta \leq 0$ .

Dataset	CIFAR10	ImageNet
Optimizer	SGD with Momentum	
Initial learning rate $\alpha$	0.01	0.1
Learning rate drop interval (epochs)	80	30
Learning rate drop factor	0.1	0.1
Momentum	0.9	0.9
Training epochs	200	100
$l_2$ regularization	0.0005	0.0001
Minibatch size	64	256
Microbatch size	8	16

Table 6: Training hyperparameters for ResNet 50 on CIFAR10 and ImageNet.

## C Supplementary material for Section 4

In this section, we discuss the setup details and additional experiment results. We first discuss the setup of each task we consider and the hyperparameter configuration of PipeMare in Appendix C.1. We then present experiment results in addition to the performance and ablation study in Section 4. In Appendix C.3, we perform a trade-off study on the number of pipeline stages; we show that up to 214 stages for the ResNet 50 and 186 stages for the 12-layer Transformer, PipeMare can demonstrate better time-to-accuracy with higher number of stages.

### C.1 Experiment setup

We discuss the details in setup for each task we consider as well as in the hyperparameter configurations for PipeMare.

**ResNet experiments.** We use a publicly available implementation<sup>6</sup> of ResNet for CIFAR10 which is reported to have good performance on CIFAR. We inherit the hyperparameters from the code repository except the initial learning rate. As the test accuracy associated with the provided learning rate does not reach 94.0, we search it with grid  $\{0.001, 0.01, 0.1\}$  to ensure the strong performance of synchronous baselines. We then uniformly apply the optimal value 0.01 to all the synchronous and asynchronous pipeline-parallel training. For the ImageNet experiment, we fully inherit the model and training configurations from the official PyTorch implementation.<sup>7</sup> For both the CIFAR10 and ImageNet dataset, we use the standard train/validation/test dataset split in the Python Torchvision library. We present the detailed model hyperparameters and training configuration in Table 6.

**Transformer experiments.** We use the Fairseq implementation for 12-layer transformer models and inherit the key hyperparameters from the Fairseq repository.<sup>8</sup> We use  $2\times$  longer learning rate linear warmup steps than in the original code repository across experiments because we observe  $2\times$  linear warmup steps can produce higher BLEU scores for both the synchronous and asynchronous runs. For both the IWSLT14 and WMT17 German to English dataset, we use beam width 5 to evaluate the BLEU score. We present the other hyperparameters in Table 7 for reproducibility.

**Hyperparameter of PipeMare.** PipeMare has three key hyperparameters for the three techniques: the number of annealing epochs for learning rate rescheduling (T1); the decay  $D$  for discrepancy correction (T2); the number of epochs (steps) for warmup epochs (T3). To compare the best model accuracy attained by different training algorithms, we following the approach used by Wilson et al. [22]—we report the best test

<sup>6</sup><https://github.com/kuangliu/pytorch-cifar>

<sup>7</sup><https://pytorch.org/>

<sup>8</sup>Fairseq repo: <https://github.com/pytorch/fairseq>



Dataset	IWSLT	WMT
Optimizer	AdamW	
Max learning rate	$5 \times 10^{-4}$	$7 \times 10^{-4}$
Label smoothing	0.1	
Dropout	0.3	0.1
Weight decay	$1 \times 10^{-4}$	0
LR linear warmup minibatches	8000	
Initial LR for linear warmup up	$1 \times 10^{-7}$	
Adam $\beta$ s	(0.9, 0.98)	
Training epochs	60	80
Minibatch size (average # of tokens)	3600	29000
Microbatch size (max # of tokens)	245	1792
# of microbatches	19	
Gradient norm clipping threshold	25	NA

Table 7: Training hyperparameters for the Transformer on IWSLT and WMT. Here, “LR” stands for learning rate.

set model accuracy attained across the hyperparameter grid. For the CIFAR10 and IWSLT14 experiments, we sweep the annealing epochs, the decay and the number of epochs sequentially. When sweep each of these parameters, we first anchor on the optimal values of the already swept hyperparameters. We then re-sweep the number of annealing epochs after sweeping the grid for the decay and the number of warmup epochs; we observe this re-sweep on the number of annealing epochs can improve the model accuracy attained by PipeMare on IWSLT14. Note for each hyperparameter configuration, we report the model accuracy as the best performance across all training epochs.

In Table 8, we present the hyperparameter grid we use as well as the optimal values (in bold) when sequentially sweeping the hyperparameters for CIFAR10 and IWSLT14 in Section 4. Note for CIFAR10, we found that warmup epochs do not further improve the statistical efficiency; we thus use 0 warmup epochs to attain the best time-to-accuracy for CIFAR10. To avoid the intensive computational overhead of tuning ImageNet and WMT, we transfer the three key hyperparameters of PipeMare from CIFAR10 and IWSLT with minimal search centered around them. Specifically, for ImageNet we use the same discrepancy correction as CIFAR10 and 10 epochs (one third of total epochs before base learning rate decayed by 10, note CIFAR10 uses 20 epochs, which is a quarter of the total epochs before learning rate decay) as annealing epochs. For WMT we used the same discrepancy correction as IWSLT and 4 epochs (16k minibatch steps, while IWSLT14 uses 12k minibatch steps) for synchronous warmup and another 4 epochs for annealing (IWSLT14 uses same epochs for synchronous warmup and annealing epochs as well). Following the optimal hyperparameter setting in IWSLT, we also use the same number of epochs for annealing epochs and warmup epochs for WMT; these PipeMare configurations for ImageNet and WMT are presented in Table 9.

## C.2 Additional experiment results

We present the additional experiment results in addition to the demonstration in Section 4. We discuss the results on ImageNet and WMT dataset in Appendix C.2.1. We then discuss supplementary results for PipeMare ablation study in Appendix C.2.2 and for the tradeoff study over number of pipeline stages in Appendix C.3. Finally, we discuss the implementation details on the simulator for our experiments in Appendix C.4.

### C.2.1 ImageNet and WMT results

In Section 4.2, we discussed the end-to-end comparison on time-to-accuracy on the ImageNet and WMT dataset. To better compare the statistical efficiency and time-to-accuracy across the pipeline training methods, we visualize the model accuracy as a function of number of epochs and of normalized time in Figure 9.

Dataset	Hyperparameters	Tuning grid	Retuning grid for # of annealing epochs
CIFAR10	Number of annealing epochs (PipeMare T1)	{10, <b>20</b> , 40, 80, 160}	–
	Discrepancy correction decay (PipeMare T1 + T2)	{0.1, <b>0.5</b> , 0.9}	{10, <b>20</b> , 40}
IWSLT14	Number of annealing epochs (PipeMare T1)	{15, <b>30</b> , 60}	–
	Discrepancy correction decay (PipeMare T1 + T2)	{0.01, <b>0.1</b> , 0.2}	{15, 20, <b>30</b> }
	Warmup epochs (PipeMare T1 + T2 + T3)	{3, 5, <b>10</b> }	{1, <b>10</b> , 20}

Table 8: Hyperparameter sweep for PipeMare to demonstrate the best model accuracy attained by PipeMare. We sweep the number of annealing epochs, the discrepancy correction decay and the number of warmup epochs sequentially. For each hyperparameter, we first sweep it with optimal values for previously swept hyperparameters if there are any. After we tune the decay and number of warmup epochs, we also re-sweep the number of annealing epochs; we found this re-sweep can be important to model accuracy in cases such as PipeMare T1 + T2 + T3 for IWSLT. We use 0 warmup epochs for CIFAR10 as we found warmup epochs does not improve the model accuracy. We bold the hyperparameter values attaining the best model accuracy in each grid.

Dataset	ImageNet	WMT
Sync warmup epochs	-	4
Discrepancy correction	0.5	0.1
Annealing epochs	10	4

Table 9: PipeMare hyperparameters on the ImageNet and WMT dataset.

For the ImageNet dataset, we can observe in Figure 9 (a) that PipeMare attains higher test accuracy than PipeDream. For the WMT dataset in Figure 9 (c), PipeMare can attain competitive test BLEU score to GPipe synchronous results while PipeDream only demonstrate 0.0 BLEU score. Regarding the time-to-accuracy comparison in Figure 9 (b) (d), we observe PipeMare attains  $2.5\times$  and  $2.6\times$  speedup in time-to-accuracy comparing to the GPipe; we observe that PipeDream fails to attain the target model accuracy in both datasets.

### C.2.2 PipeMare ablation study

**Ablation study: a different number of pipeline stages.** In Section 4.3, we perform ablation study with 214 and 186 pipeline stages respectively for CIFAR10 and IWSLT. In Figure 10 we demonstrate the ablation study with 107 and 93 stages for CIFAR10 and IWSLT. We observe that the learning rate rescheduling, discrepancy correction and warmup epochs can demonstrate similar contribution to the statistical efficiency and time-to-accuracy as in Section 4.3.

**Discrepancy correction for ResNet 152.** In Section 4.3, we demonstrate discrepancy correction (T2) can improve the model accuracy on ResNet 50 and Transformer for CIFAR10 and IWSLT. In this section, we demonstrate that discrepancy correction can also contribute to preventing divergence for models with larger number of stages. More concretely, in Appendix C.2.2, we show that PipeMare T1 (only with learning rate rescheduling) diverge for ResNet 152 on CIFAR10 with 150 pipeline stages. By additionally applying discrepancy correction, we observe that PipeMare converges and achieve matching test accuracy to GPipe training in a fixed number of epochs after the first learning rate drop after 80 epochs.

### C.2.3 Hyperparameter sensitivity studies

We empirically demonstrate the sensitivity of model accuracy to the three key hyperparameters in PipeMare.

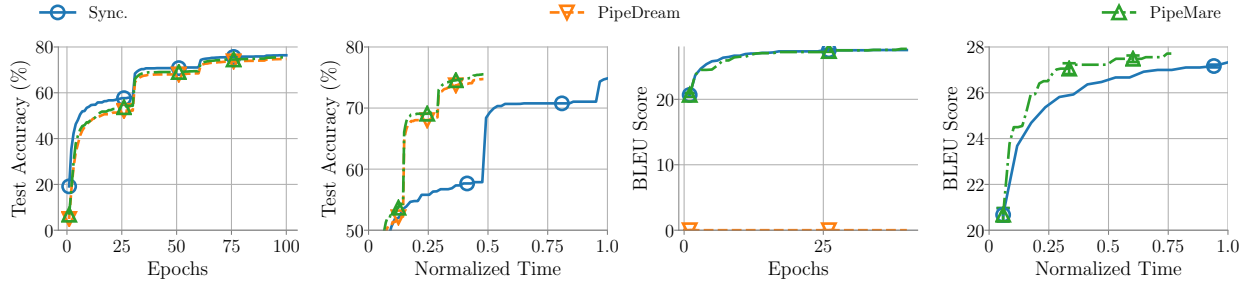


Figure 9: The statistical performance and time-to-accuracy attained by different pipeline training methods on ImageNet and WMT. In (a) (c), we observe PipeMare can attain higher model accuracy for both ImageNet and WMT, being competitive to GPipe within the same number of epochs. In (b) (d), we can see PipeMare achieves time-to-accuracy speedup over GPipe while PipeDream fails to achieve the target model accuracy. Note for WMT, we observe PipeDream attains BLEU score close to 0.

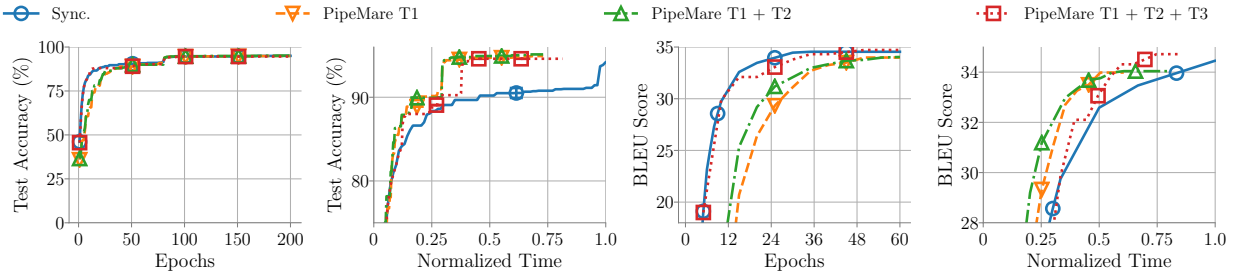


Figure 10: Tradeoffs when incrementally combining PipeMare techniques (T1, T2, and T3). We set the number of pipeline stages in the ResNet50 and the 12-layer Transformer models to 107 stages and 83 which is the number of pipeline stages that would occur if each model weight is treated at its own stage. This simulates a very fine-granularity of pipeline parallelism to test the limits of each technique at an extreme.

**Sensitivity to annealing epochs.** One key hyperparameter for improving convergence using Heuristic 1 is the number of annealing epochs  $K$ . We further study here the sensitivity of model accuracy (loss) with respect to the number of annealing epochs in ResNet and Transformer model. As shown in Figure 12, we observe that different model may require a different number of annealing epochs for optimal test performance. Specifically, we can see that the ResNet and Transformer model prefers small and large number of annealing epochs respectively.

**Sensitivity to correction decay.** A right choice of correction decay is important to stabilizing the training and speed up the convergence. As shown in Figure 13, a proper correction decay  $D$  ( $\leq 0.2$ ) can speed up the convergence of Transformer while an improper  $D$  can result in even worse result than those without corrections. In other words, simply reusing the momentum buffer in SGD updates for correcting the parameters during backward could not fulfill the purpose of approximating the parameters used during forward. Therefore, an extra memory buffer and accumulation  $\gamma$  is needed for each stage, which adds additional 25-33% of memory to the total weight memory (e.g., in Adam, we have master weight, gradient, momentum, and norm, totally four copies of weight memory).

**Sensitivity to warmup epochs.** In Appendix A, we show that under the same memory constraint, synchronous training (GPipe) has a hardware utilization about 0.3 of fully pipelined asynchronous training. Therefore, when asynchronous training takes more than 3.3 times of epochs to converge to a certain loss

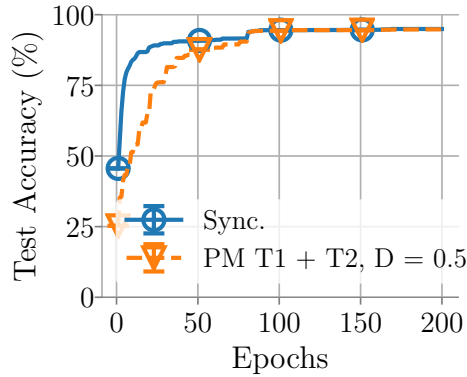


Figure 11: We observe ResNet 152 on CIFAR20 diverges when only using learning rate rescheduling (T1). Discrepancy correction is necessary to prevent divergence for ResNet 152 on CIFAR10; we observe PipeMare with discrepancy correction (T1 + T2) attains matching performance to GPipe synchronous training.

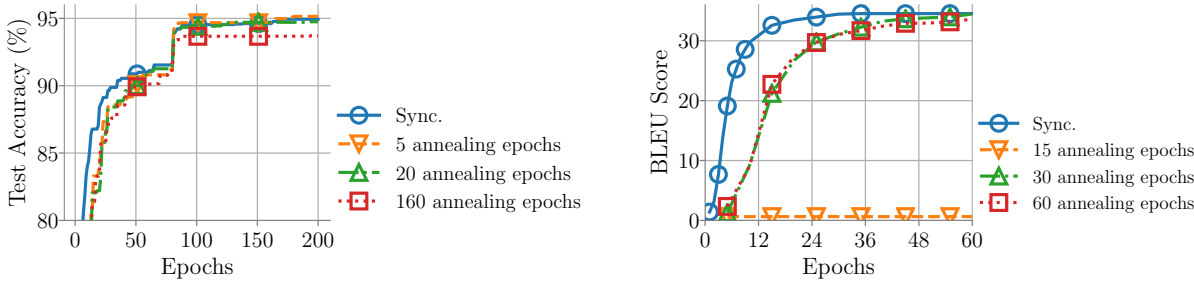


Figure 12: Sensitivity of model accuracy to the number of annealing epochs. We observe that choosing the number of annealing epochs can be important to achieving model accuracy matching synchronous training.

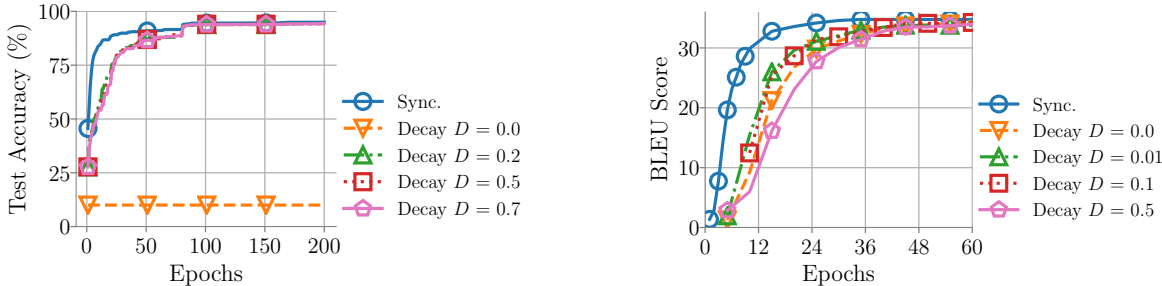


Figure 13: Sensitivity of model accuracy to the decay  $D$  for discrepancy correction. We notice that the decay value can have an impact on the convergence speed. For example, it requires a decay smaller than 0.5 to converge faster than without discrepancy correction while 0.5 can demonstrate test accuracy matching that attained by synchronous training.

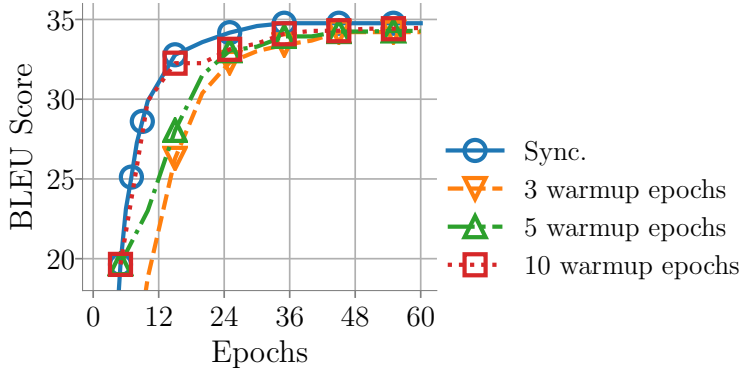


Figure 14: Sensitivity of model accuracy to the number of synchronous warmup epochs on IWSLT. We observe a time-to-accuracy tradeoff in using warmup epochs: large number of warmup epochs can harm the throughput while converging to target model accuracy with less number of epochs. It is important to properly configure the number of warmup epochs to attain optimal time-to-accuracy speedups.

than synchronous training (which often happens during the beginning of the training due to low statistical efficiency), it is worth using synchronous training instead of asynchronous training, and vice versa. In Appendix C.2.3, we demonstrate the time-to-accuracy speedup with different number synchronous training to reach within approximately 1% relative difference to the best test BLEU score attained by asynchronous training. We observe that the best speedup is achieved with 5 synchronous training epochs. More synchronous training epochs degrade the time-to-accuracy due to the lower throughput of synchronous training compared to synchronous training.

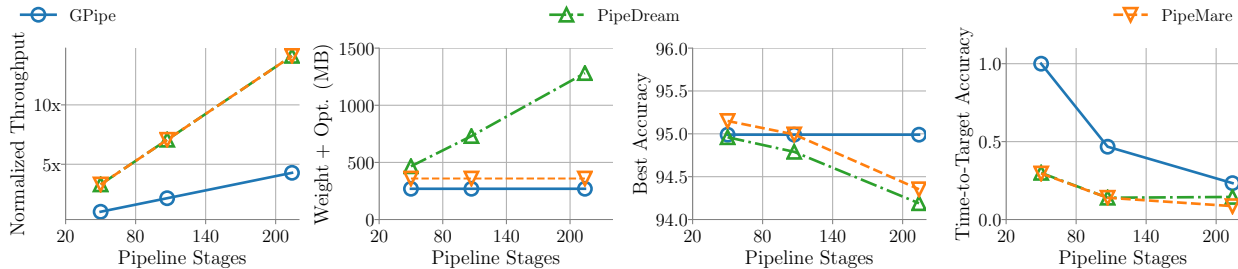


Figure 15: The impact of the number of pipeline stages on throughput, weight memory, final model quality, and time-to-quality across different pipeline parallel training methods on a ResNet 50 for image classification with the CIFAR10 dataset. Unlike PipeMare, GPipe and PipeDream suffer hardware costs (either throughput or weight memory) proportional to the number of pipeline stages. Still, PipeMare achieves a final model quality competitive with the best technique. In (d) PipeDream is unable to achieve an acceptable final model quality resulting in an infinite time-to-quality metric.

### C.3 Trade-off study on the number of pipeline stages

In pipeline-parallel training, the pipeline depth or the number of stages plays an important role in the statistical and hardware efficiency. To better understand how the pipeline depth interacts with the time-to-accuracy performance, we study the memory footprint, throughput, model accuracy and time-to-accuracy for PipeMare with different number of pipeline stages. We show that increasing the number of stages can boost the hardware efficiency while minimally impact the statistical efficiency; this translates to better time-to-accuracy for higher number of stages, up to the maximal number stages we use for experiments.

Our experiment evaluate up to 214 stages for ResNet on CIFAR10 and 186 stages for Transformer on IWSLT14. In this experiment, we tune the hyperparameter for PipeMare with 107 and 93 groups for the CIFAR10 and IWSLT14 dataset as discussed in Table 8 in Appendix C.1. We then use the same PipeMare hyperparameter configurations for other number of stages.

**Evaluation results** We demonstrate the impact of number of stages on the performance of PipeMare in Figure 2 for IWSLT14 in Section 2 and in Figure 15 for CIFAR10. For up to 214 stages for ResNet on CIFAR10 and 186 stages for Transformer on IWSLT14, increasing the number of stages can (almost) linearly increase the system throughput for GPipe, PipeDream and PipeMare. For the memory to store model weights, both GPipe and PipeMare stays constant while increasing linearly for PipeDream due to weight stashing. We also observe that an increased number of stages has minimal impact on the best performance attained by PipeMare, while it strongly influence the test BLEU score attained by PipeDream. In Figure 2 (d) and Figure 15 (d), we can see that increasing the number of stages can improve the time-to-accuracy. We note across the different number of stages we study, PipeMare attains better time-to-accuracy than GPipe; PipeDream on the other hand, fails to attain the targeted test BLEU score we use on IWSLT14.

## C.4 Simulator implementation details

We implement PipeMare using a simulator based on PyTorch. We maintain a queue of weights for each individual pipeline stage to simulator the pipeline behavior for each minibatch / microbatch. To further scale up the simulator for larger model / dataset with faster simulation, we are excited about single machine speed optimization and distributed implementations of the simulator as future work. We hope our simulation based exploration can trigger more study and production implementation of asynchronous pipeline training for the new generation of machine learning accelerators.

## D Statistical Efficiency and Recompute

In pipeline-parallel training, to compute the gradient in a pipelined fashion, the activation memory needs to be stored for each batch of data at every pipeline stage. For fine-grained pipeline-parallel training, this can results in significantly increased memory footprint. To reduce the memory incurred by activations, the activation recomputation technique [3, 9] has been proposed for training deep neural networks. We first discuss the recomputation model in asynchronous pipeline-parallel training in appendix D.1. We then demonstrate in appendix D.2 that PipeMare with recomputation can attain matching / competitive model accuracy while using less memory footprint comparing to PipeMare without recomputation.

### D.1 Asynchronous pipeline-parallel recomputation

When running with asynchronous pipeline parallelism, adding recompute adds additional delay paths to the computation, since now the backward pass depends not only on a single delayed weight value but also on delayed recomputed activations, each of which may have a different delay from the delay used for the backward-pass weights. We can model this formally as

$$w_{t+1} = w_t - \alpha \nabla f_t(u_{\text{fwd},t}, u_{\text{bkwd},t}, u_{\text{recomp},t}),$$

where now  $u_{\text{recomp},t}$  denotes the delayed version of the weights used for recomputing activations in the backward pass for the  $t$ th gradient microbatch. Just as for the other delayed weights, we define this in terms of a fixed delay as

$$(u_{\text{recomp},t})_i = (w_{t-\tau_{\text{recomp},i}})_i$$

where now  $\tau_{\text{recomp},i}$  is a fixed delay that affects weights used for recomputation in the  $i$ th layer. Given this definition, there is a natural way we can extend the discrepancy correction of T2 to apply to these new recomputed activations.

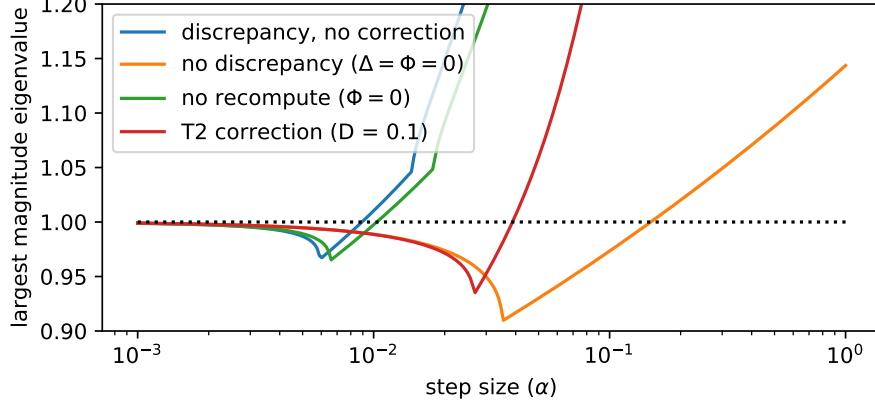


Figure 16: Effect of discrepancy correction on the quadratic model when recompute is used for a model with  $\Delta = 10$ ,  $\Phi = -5$ ,  $\tau_{\text{fwd}} = 10$ ,  $\tau_{\text{bkwd}} = 1$ ,  $\tau_{\text{recomp}} = 4$ , and  $\lambda = 1$ . Forward-backward delay discrepancy (blue) increases the largest magnitude eigenvalue of the companion matrix, just as in the no-recompute case (green). Discrepancy correction with  $D = 0.1$  (red) reduces the largest magnitude eigenvalue; this eigenvalue is closer to that attained without delay discrepancy (orange).

**T2 for Recompute:** *Instead of the assignment of  $u_{\text{recomp}}$  above, set*

$$(u_{\text{recomp},t})_i = (w_{t-\tau_{\text{recomp}},i})_i - (\tau_{\text{fwd},i} - \tau_{\text{recomp},i}) \delta_{t,i},$$

where  $\delta_{t,i}$  is the same weight-trajectory accumulator used to correct  $u_{\text{bkwd},t}$  in T2.

**The theory.** To model delay discrepancy with recombination in the quadratic model, we now assume gradient samples of the form

$$\begin{aligned} \nabla f_t(u_{\text{fwd},t}, u_{\text{bkwd},t}) &= (\lambda + \Delta) \cdot w_{t-\tau_{\text{fwd}}} \\ &\quad - (\Delta - \Phi) \cdot w_{t-\tau_{\text{bkwd}}} \\ &\quad - \Phi w_{t-\tau_{\text{recomp}}} - \eta t \end{aligned}$$

where  $\tau_{\text{fwd}} > \tau_{\text{recomp}} > \tau_{\text{bkwd}}$  are now three different delays, and  $\Phi$  is now a constant that measures the sensitivity of the gradients to discrepancy between the recomputed weights and the backward-pass weights. As before, we can think of this as the natural first-order (linear) approximation of  $\nabla f_t$ ; it can model any affine function of  $u_{\text{fwd},t}$ ,  $u_{\text{bkwd},t}$ , and  $u_{\text{recomp},t}$  that is consistent with the curvature  $\lambda$  when  $u_{\text{fwd},t} = u_{\text{bkwd},t}$ . If  $\Phi = 0$ , we recover our original no-recomputation setting, whereas for large-magnitude values of  $\Phi$ , even a small delay discrepancy in recombination could cause a large effect on the gradient samples.

It is straightforward to see that the characteristic polynomial of the companion matrix here will be

$$\begin{aligned} p(\omega) &= (\omega - 1)(\omega - \gamma)\omega^{\tau_{\text{fwd}}} \\ &\quad + \alpha(\lambda + \Delta)(\omega - \gamma) \\ &\quad - \alpha(\Delta - \Phi)\omega^{\tau_{\text{fwd}} - \tau_{\text{bkwd}}}(\omega - \gamma) \\ &\quad + \alpha(\Delta - \Phi)\omega^{\tau_{\text{fwd}} - \tau_{\text{bkwd}}}(\tau_{\text{fwd}} - \tau_{\text{bkwd}})(1 - \gamma)(\omega - 1) \\ &\quad - \alpha\Phi\omega^{\tau_{\text{fwd}} - \tau_{\text{recomp}}}(\omega - \gamma) \\ &\quad + \alpha\Phi\omega^{\tau_{\text{fwd}} - \tau_{\text{recomp}}}(\tau_{\text{fwd}} - \tau_{\text{recomp}})(1 - \gamma)(\omega - 1). \end{aligned}$$

While the complexity of this polynomial makes it difficult to prove a tight result like Lemma 1, we can still analyze its spectral radius empirically, as we did for the non-recompute case in the main body of the paper.

Figure 16 shows this analysis. Here we see that, just as in the case without recompute, delay discrepancy correction increases the range of step sizes over which the quadratic model is stable, and brings the behavior of the model closer to the no-delay-discrepancy case.

## D.2 Statistical efficiency and recompute

To study the impact of recompute over statistical efficiency, we study the model accuracy attained by PipeMare with recompute on CIAFR10 and IWSLT. We observe that 1) as discussed in Appendix D.1, discrepancy correction can be important to the stability of asynchronous training with recompute; 2) with different number of gradient checkpoints for recompute, PipeMare in general attains competitive or matching model accuracy to that attained by PipeMare without recompute.

**Setup.** In our experiment, we set gradient checkpoints at the natural module boundaries defined by skip connections. More concretely, ResNet uses residual connection between groups of convolutional layers while Transformer uses skip connections for both the multiple headed attention and feedforward modules. Following this principle, we use  $\{2, 4, 17\}$  checkpoints and  $\{2, 12, 31\}$  checkpoints to segment the models respectively for ResNet 50 and 12-layer Transformer model. To fully study the impact of recompute, we consider different combination of the key techniques in PipeMare. Specifically we consider T1, T1 + T2 and T1 + T2 + T3 for IWSLT; we consider only T1 and T1 + T2 for CIFAR 10 as warm up epochs (T3) does not bring observable model accuracy improvement on CIFAR10.

**Importance of discrepancy correction.** In Figure 17 and Figure 18, we plot the model accuracy attained by PipeMare with recompute using different number of gradient checkpoints on CIFAR10 and IWSLT. For the CIFAR10 case in Figure 17, using recompute does not affect the model accuracy attained with discrepancy correction (PipeMare T1 + T2) and without discrepancy correction (PipeMare T1). However for the IWSLT case in Figure 18, without discrepancy correction (PipeMare T1), training with recompute in the asynchronous setting can be unstable. E.g. training with 2 gradient checkpoints fails to attain BLEU higher than 10.0 while it diverge in the middle of training for 12 gradient checkpoints. When we apply the discrepancy correction in the middle and right plot of Figure 18, we can observe that PipeMare with different number of gradient checkpoints can achieve matching model accuracy to training without recompute. These observations indicate that discrepancy correction is important to the stability of training with recompute.

**Statistical efficiency with recomputation.** In Figure 17 (right) and Figure 18 (middle, right), we can see that with discrepancy correction, PipeMare asynchronous pipeline-parallel training can consistently attain strong model accuracy on both CIFAR10 and IWSLT. This further emphasizes that PipeMare can be orthogonally combined with recompute to attain strong model accuracy with significantly reduced activation memory footprint.

## E Hogwild! asynchrony

Asynchrony has been studied in various settings to accelerate the training of machine learning models [15, 11]. We ask the question of whether our proposed heuristic can go beyond the asynchronous pipeline setting with fixed gradient delay pattern, and accelerate training in classical asynchronous settings with stochastic gradient delay. In this section, we show that our learning rate rescheduling heuristic can also improve the model accuracy attained by training under the Hogwild!-style stochastic asynchrony [15, 5]. We first discuss the Hogwild!-style stochastic asynchrony model and then dive into the detailed experiment results.

**Stochastic asynchrony model** Hogwild!-style asynchrony considers a setting where the model is updated with a staled gradient. Specifically, the update of SGD algorithm over an objective function  $f(w)$  can be written as

$$w_{t+1} = w_t - \alpha \nabla f_{t-\tau}(w_{t-\tau}) \tag{16}$$



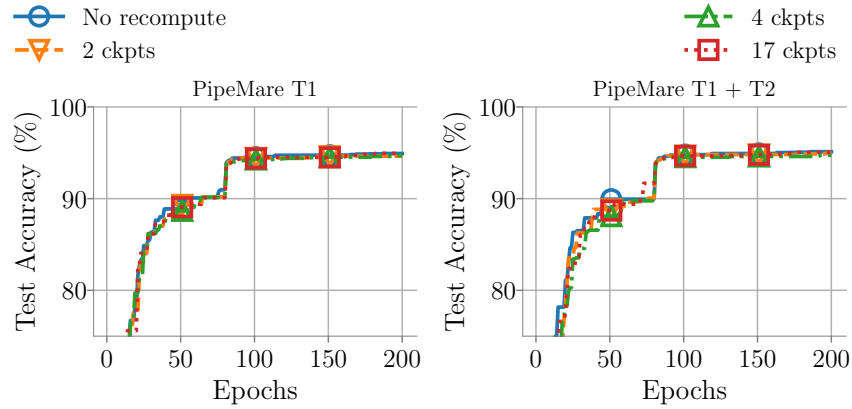


Figure 17: The statistical performance of recompute with different number gradient checkpoints on CIFAR10. We observe that with different number of gradient checkpoints, PipeMare with recompute can match the model accuracy attained by PipeMare without recompute. This indicates that recompute can significantly save the memory for storing activations with minimal influence on the attained model accuracy.

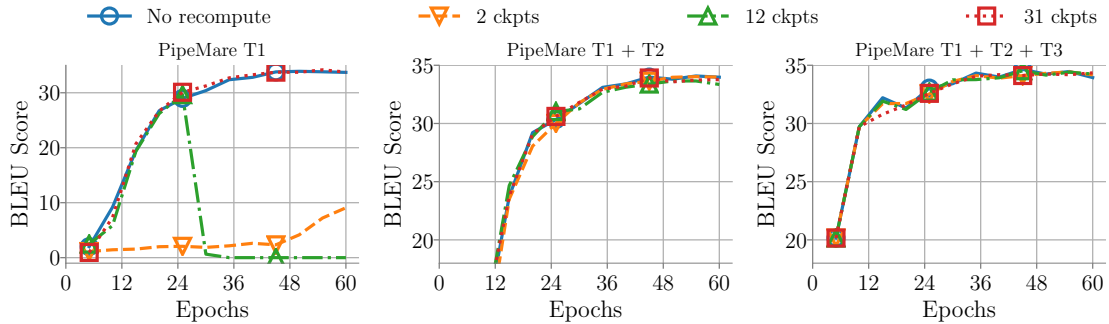


Figure 18: The statistical performance of recompute with different number gradient checkpoints on IWSLT. We observed in the left plot that when only using learning rate rescheduling (T1) without discrepancy correction, recompute can unstable training with 2 and 12 gradient checkpoints. After applying discrepancy correction (T2) in the middle and right plots, we observe that with different number of gradient checkpoints, PipeMare with recompute can match the model accuracy attained by PipeMare without recompute. This indicates the importance of discrepancy correction to attaining stable recompute in PipeMare.

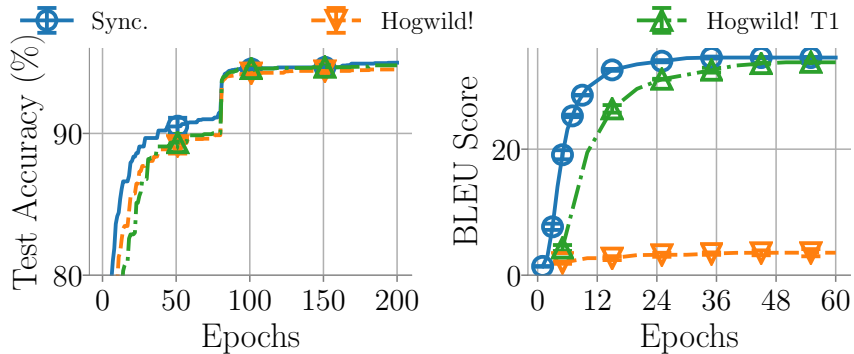


Figure 19: Test performance of CIFAR10 ResNet (left) and IWSLT14 Transformer (right) under the Hogwild!-style asynchronous training. By using the learning rate rescheduling heuristic for asynchronous training, we can achieve test performance matching those attained by synchronous training. Comparing to asynchronous training without learning rate rescheduling, applying the rescheduling heuristic can attain better test performance after the same number of training epochs.

where  $w_t \in \mathbb{R}^d$  is the model iterate while  $\nabla f_t(W_t)$  is the stochastic estimate of the gradient  $\nabla f(w_t)$  at time step  $t$ . The  $\tau_t$  here is a random variable describing the delay of the gradient; this random variable can model the delay of gradients due to the network transmission in distributed asynchronous training [11] or asynchronous model update in the shared memory settings [15].

We consider a variant of the original Hogwild!-style asynchrony model with different delays for different stages; this stage specific gradient delay setting is studied in our fixed delay asynchronous pipeline training in Section 3. In particular, the model update for each stage can be characterized by

$$w_{i,t+1} = w_{i,t} - \alpha[\nabla f_{t-\tau_i}(w_{t-\tau_i})]_i \quad (17)$$

where  $\tau_i$  is the stochastic gradient delay for the  $i$ -th stage and  $[\nabla f_t(w_{t-\tau_i})]_i$  describes the gradient dimensions corresponding to the  $i$ -th stage.

In our variant of the Hogwild!-style gradient delay  $\tau_i$ , we sample from truncated exponential distributions following the existing study in asynchronous training [14]; this truncated exponential distribution is the maximum entropy distribution. We use the exponential distribution truncated at  $\tau_{\max}$  uniformly for different stages to make sure we have bounded delay of the gradient. To model the different level of gradient delay for different stages, we use sampling distributions with different expectation values.

**Evaluation results** To demonstrate that our learning rate rescheduling rule can also improve the model accuracy for training under Hogwild!-style asynchrony, we evaluate with the ResNet50 model on the CIFAR10 dataset and the Transformer model on the IWSLT14 German to English translation task. In our experiment, we use the maximal number of stages with at least one model weight in each group, which is also used in our pipeline training experiments in Section 4.3. Specifically, we use 107 and 93 stages for the ResNet and Transformer model respectively. We thus also inherit the optimal configuration for annealing epochs from the experiment on PipeMare only with learning rate rescheduling (PipeMare T1) in Section 4.3. As shown in Figure 19, we can observe that asynchronous training without learning rate rescheduling attains 94.51% test accuracy and test BLEU score 3.6 respectively for ResNet and Transformer. By applying learning rate rescheduling as described in Section 3.1, we improve the test accuracy to 94.80% and test BLEU score 33.8 for asynchronous pipeline-parallel training for the ResNet and Transformer model. These observations indicates that our learning rate rescheduling heuristics can also improve the test performance of training under Hogwild!-style asynchrony.